Evaluation of CFRP reinforced prestressed concrete beams for shear behavior

by

Yassin Abbas

B.S., Kansas State University, 2020

A THESIS

submitted in partial fulfillment of the requirements for the degree

MASTER OF SCIENCE

GE Johnson Department of Architectural Engineering and Construction Science
Carl R. Ice College of Engineering

KANSAS STATE UNIVERSITY
Manhattan, Kansas

2022

Approved by:
Major Professor
Bill Zhang

Abstract

Fiber-reinforced polymer (FRP) can be effectively utilized in structures as rods, sheets, bars, and tendons due to its high strength-to-weight ratio, non-corrosiveness, non-magnetic properties, and its flexibility. FRPs include carbon fiber-reinforced polymers (CFRPs), aramid fiber-reinforced polymers (AFRPs), and glass fiber-reinforced polymers (GFRPs). Previous studies have investigated these materials under various load conditions and in a variety of structures, including prestressed concrete beams reinforced with CFRP, which has the highest tensile modulus out of all the FRP varieties.

The increasing popularity of FRP as a reinforcement particularly as prestressing tendons in concrete structures is prompting research to more accurately predict the behavior of such structures under various types of loading and boundary conditions. Although many studies have investigated the flexural behavior of beams reinforced with FRP, few studies have focused on their complex shear behavior. Design guidelines in the U.S. such as ACI440.4R-04 and AASHTO 2018 have been published to support the design of structures using FRP. The objective of this thesis was to evaluate these guidelines for accuracy in predicting nominal shear capacity using prestressed concrete beams reinforced with CFRP. This study also aimed to offer alternative solutions to improve calculations of nominal shear capacity for prestressed beams reinforced with CFRP tendons.

Table of Contents

List of Figures

List of Tables

Acknowledgments

To my loving family for supporting me and my supportive professors for guiding me.

Chapter 1 – Introduction

Fiber-reinforced polymers (FRPs) have gained significant research attention for their use with or as a substitute for steel in reinforced concrete structures. Their high strength-to-weight ratio, non-corrosiveness, non-magnetic properties make them a good reinforcement in concrete. Their flexibility means that they can be utilized as rods, sheets, bars, or tendons. FRPs include carbon fiber-reinforced polymers (CFRPs), aramid fiber-reinforced polymers (AFRPs), and glass fiber-reinforced polymers (GFRPs), as shown in Figure 1.1.

Figure 1.1. FRP Configurations (Dolan et al., 2001)

FRP selection depends on mechanical properties, such as the modulus of elasticity. As shown in Figure 1.2, CFRP has the highest modulus, followed by steel, AFRP, and GFRP. However, these mechanical properties can vary depending on the method that they are manufactured.

Figure 1.2. Stress and Strain Curves for Various Types of Tendons (Dolan, 1990)

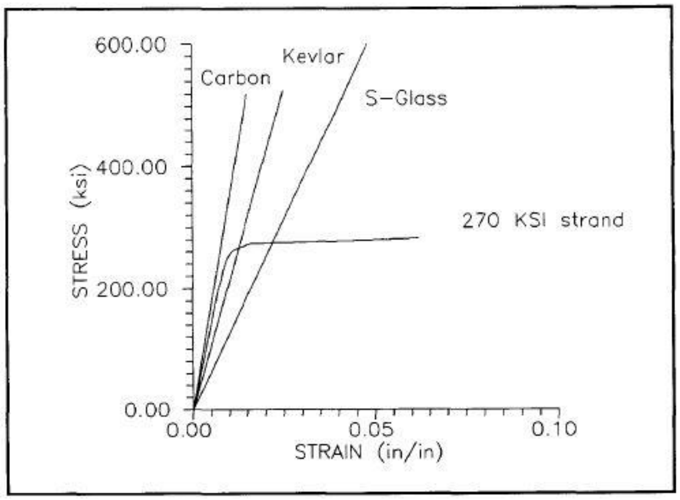

FRP was introduced in the 1930s in the form of glass fibers mixed with cement (Dolan & Hamilton III, 2001). In the 1950s and 1960s, the United States Army Corps of Engineers began testing the material for reinforced and prestressed concrete (Dolan & Hamilton III, 2001; Mather & Tye, 1955; Pepper & Mather, 1959; Wines et al., 1966). In 1978, Strabag-Bue and Bayer produced GFRP and an anchor system for post-tension application, and in 1983, AkzoNobel and Hollandsche Beton Groep (HBG) in the Netherlands developed AFRP prestressing tendons. Around that time, the Japanese began developing FRP application in concrete structures and production methods for FRP reinforcement. In 1988, Iyer and Kumarswamy, with the support of the Florida Department of Transportation (FDOT), developed a new glass fiber tendon to investigate the prestressing application of glass fiber tendons for bridge and marine substructures. In 1989, Dolan investigated the prestressing of AFRP (Kevlar), the results of which were discussed in the first International Symposium for FRP in Reinforced Concrete Structures (FRPRCS-1) (ACI 440.4R, 2004; Nanni & Dolan, 1993) and in a publication called *Japanese Society of Civil Engineering* (JSCE, 1997). Continued interest in FRP reinforcement in concrete structures has motivated research to increase understanding of FRP behavior.

The first guideline for FRP reinforcement in prestressed concrete buildings was established in 1993 by JSCE under a Japanese Ministry of Construction's research and development project. The Canadian Standard Association then produced two standards that contained FRP prestressing provisions: CSA S6-00 and CSA S806-02. The second edition of CSA S806-02 was published in 2017 as CSA S806-12, and it provided requirements for the design and evaluation of building components made of FRP and reinforced with FRP materials.

The merging of Euro-International Committee for Concrete (CEB) and the Federation Internationale de la Precontrainte (FIP) in 1998, resulted in a new task group in Europe, the Federation Internationale du Béton (*fib*). Task Group 9.3 of *fib* developed design guidelines for concrete structures reinforced, prestressed, and strengthened with FRP. Task Group 9.3 was later combined with Task Group 5.1 to continue to develop FRP design guidelines, including *fib* 90 for externally applied FRP reinforcement for concrete structures and *Prospect for New Guidance in the Design of FRP Structures* (2019).

In 1962, the American Association of State Highway and Transportation Officials (AASHTO) initiated and funded the National Cooperative Highway Research Program (NCHRP). In 2013, the project group NCHRP Project 12-97 led by the University of Houston and funded by AASHTO was assigned to develop design and material specifications in the AASHTO Load and Resistance Factor Design (LRFD) for concrete bridge beams prestressed with CFRP systems (NCHRP, 2019). The findings of NCHRP Project 12-97 were presented in the NCHRP research report 907 and the first edition of the AASHTO *Guide Specifications for the Design of Concrete Bridge Beams Prestressed with Carbon Fiber Reinforced Polymer (CFRP) Systems* (2018). Another guide specification for concrete reinforced with GFRP, called AASHTO GFRP-2, was developed in 2009, with a second edition released in 2018. In 2004, the

American Concrete Institute (ACI) established a committee (ACI 440) to study the current state of design, development, and research of prestressing concrete structures with FRP tendons. In 2004, the committee presented the guideline in *Prestressing Concrete Structures with FRP Tendons* (ACI 440.4R-04). Michigan Department of Transportation (MDOT), worked with Lawrence Technology University to develop non-corrosive CFRP to enhance the design, construction, and durability of highway bridge beams to increase resistance to the Michigan weather (Grace & Bebawy, 2019). The report was submitted in 2019, the same year that MDOT created a guideline for designing prestressed beams reinforced with CFRP.

Multiple projects have utilized FRP for construction. In 1988, the Marienfelde Bridge in Berlin, Germany, was the first structure to use external unbonded prestressing tendons (ACI 440, 2004; Wolff & Miessler, 1989). Later, the Badische Anilin und SodaFabrik (BASF) bridge in Ludwigshafen, Germany, was constructed using four CFRP internally unbounded post-tension tendons in conjunction with steel tendons (Zoch et al., 1991; ACI 440, 2004). In 1993, FRP prestressing tendons were used to construct a bridge in Calgary, Canada, followed by a second bridge in Headingly, Manitoba, in 1997 (ACI 440, 2004; Dolan & Hamilton III, 2001; Rizkalla & Tadros, 1994). In 2001, prestressing CFRP tendons were used in the construction of a bridge called Bridge Street in Southfield, Michigan. In addition to the many other projects described in the report from Lawrence Technology University (Grace & Bebawy, 2019), multiple bridges, cooling towers, and other structures were constructed throughout Europe, as presented in the *Prospect for New Guidance in the Design of FRP* (CEN/TC250, 2016).

The objective of this thesis was to evaluate these guidelines for accuracy in predicting nominal shear capacity using prestressed concrete beams reinforced with CFRP under shear.

This study also aimed to offer alternative solutions to improve calculations of nominal shear capacity for prestressed beams reinforced with CFRP tendons.

Chapter 2 – Literature Review

The references discussed in this chapter are about the shear behavior of prestressed concrete beams reinforced with FRP tendons. The following is a summary of the references and the conclusions in them.

2.1 Shear Behavior of Concrete Beams Prestressed with FRP Tendons

Park and Naaman (1999) tested two series of rectangular concrete beams. The first series included nine beams without stirrups, where five beams were prestressed with CFRP and four were prestressed with steel. One beam with CFRP tendons was made of fiber-reinforced concrete with discontinuous steel fibers. The second series included eight beams where six beams were prestressed with CFRP, one non-prestressed beam reinforced with CFRP, and one beam prestressed with steel. One of the six beams was not reinforced with stirrups, and it included steel fibers.

The materials used were seven-wire CFRP tendons manufactured by Tokyo Ropes Company. These tendons were 0.3125 inches (7.935 mm) in diameter with a specified stress of 307 ksi (2117 MPa) and tensile modulus of 19,900 ksi (137.2 GPa) or 0.5 inches (12.7 mm) in diameter with a specified stress of 315 ksi (2172 MPa) and tensile modulus of 21,000 ksi (145 GPa). The steel tendons had diameters of 0.375 and 0.5 inches (9.52 mm and 12.7 mm) and were grade 270 ksi (1862 MPa) with a tensile modulus of 29,000 ksi (200 GPa). No. 2 round steel bars, grade 40 ksi (276 MPa), were used for the stirrups. The steel fibers were hooked fibers measuring 1.18 inches (30 mm) in length and 0.02 inches (0.51 mm) in diameter. Type III cement, natural sand, and crushed limestone aggregate (maximum 0.375 inches (9.52 mm)) were used for the concrete mixture. All the beams were simply supported and the load was at the center of the beam, as shown in the illustrated test setup and beam cross section in Figure 2.1.

Figure 2.1. Test Setup (Park & Naaman, 1999)

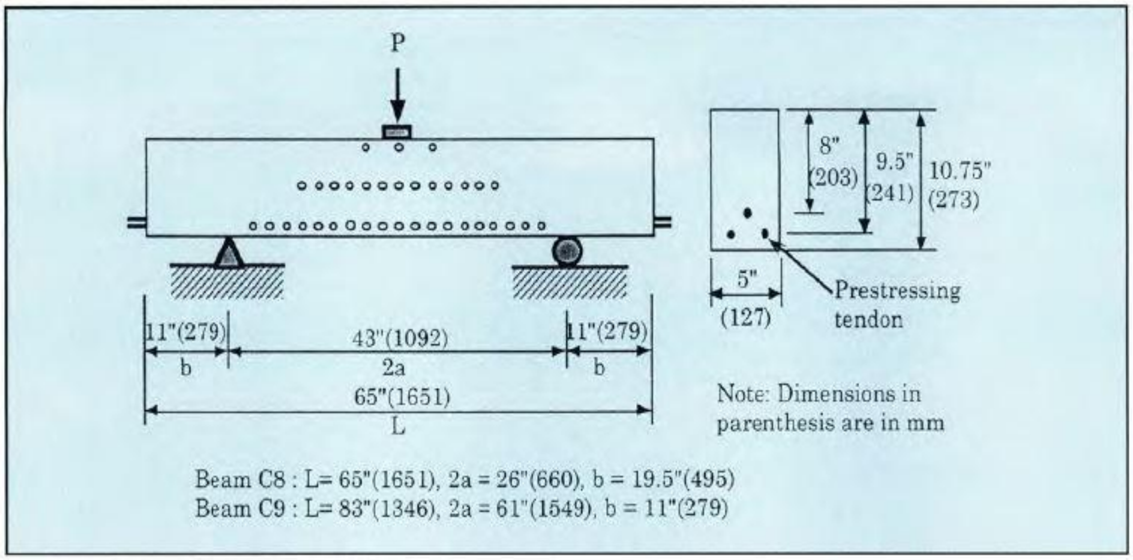

The researchers concluded that poorly designed beams prestressed with CFRP could uniquely fail in a shear-tendon rupture. The low transverse resistance and brittle behavior of CFRP tendons caused premature failure in the tendons due to the dowel shear at the shear cracking plane. The ultimate shear capacity of beams prestressed with CFRP was 15% lower than steel. The shear-tendon rupture failure mode happened in beams reinforced by prestressed CFRP along the flexural-shear cracking plane even when the effective prestressing ratio is as low as 40% and the amount of stirrups satisfies ACI 318-95. The initial portion of the load-deflection curve for both CFRP and steel prestressed concrete beams subjected to center point loading with shear span-to-depth ratio of 2.5 was not affected by the difference of the longitudinal reinforcement properties. Increasing the shear-to-depth ratio from 1.5 to 3.5 decreased shear capacity but increased shear ductility. Similarly, increasing the number of shear stirrups increased the shear capacity, and increasing the concrete compressive strength increased the shear strength slightly but increased the deflection significantly (Park & Naaman, 1999).

2.2 Shear Strength of Concrete Beams Prestressed with CFRP Cables

Mirpayam Nabipaylashgari (2012) tested eight beams in four groups. In each group, one beam was reinforced with stirrups and the other was not. The first three groups were tested under four-point bending with different span-to-depth ratios, whereas the last group was under uniform load. The beam setups and cross sections are presented in Figure 2.2 and Figure 2.3, respectively.

Figure 2.2. Beams without Stirrups & Beams with Stirrups (Nabipaylashgari, 2012)

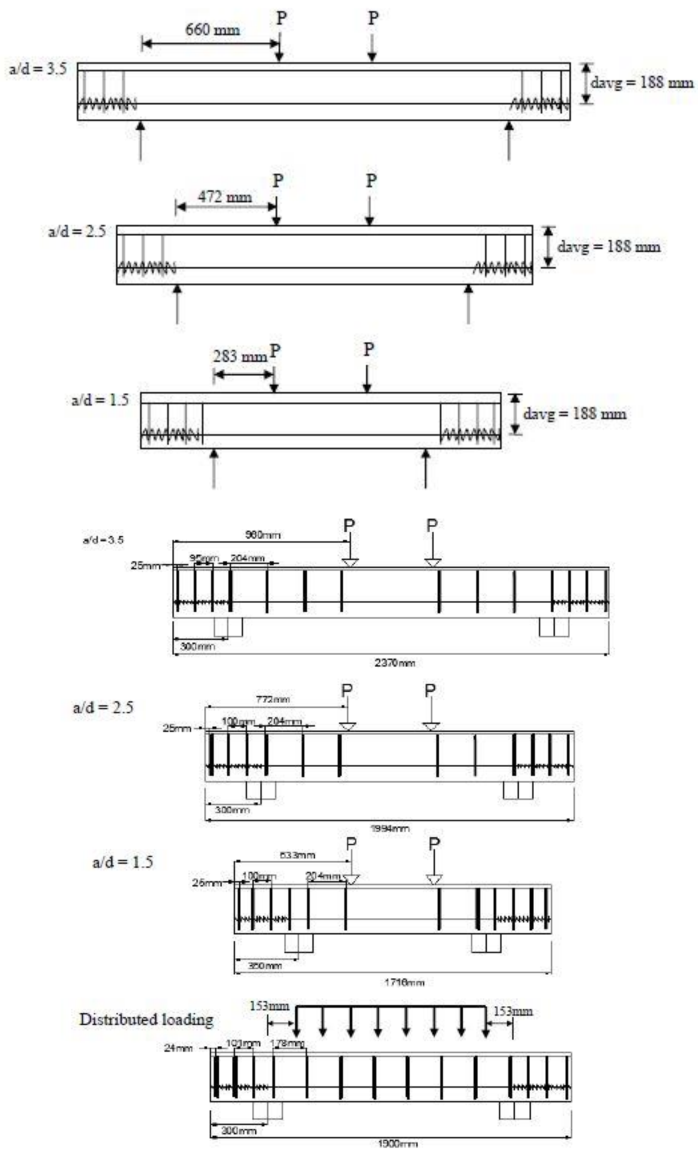

Figure 2.3. Beam Cross Section (Nabipay & Svecova, 2014)

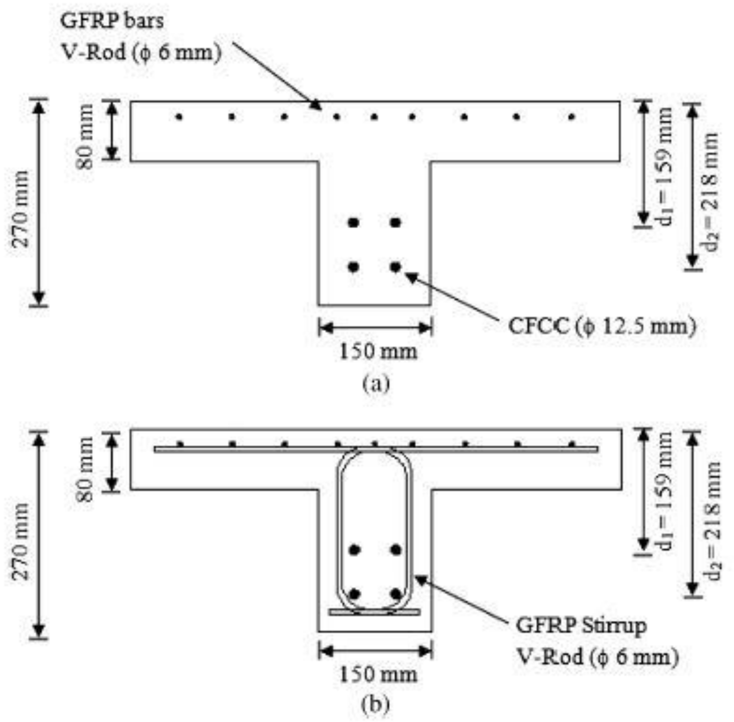

This study used CFRP cables manufactured by Tokyo Ropes called CFCC for the longitudinal prestressed reinforcement. Cable diameter was 12.5 mm, ultimate tensile stress was 2100 MPa, and tensile modulus was 136 GPa. The GFRP transverse reinforcement and compression flexural reinforcement were manufactured by Pultrall, with rebar diameters of 6 mm, ultimate tensile stress of 827 MPa, and tensile modulus of 40.8 GPa.

Results showed that beams with a span-to-depth ratio less than 2.5 had increased shear capacity and decreased deformability. The increase in shear capacity was due to arch action that occurs when beams are subjected to a low span-to-depth ratio. Moreover, increasing the number of stirrups had no effect on the shear capacity of the beams, but arch action caused the strain of the longitudinal reinforcement and the angle of inclination to increase. Comparatively, beams with a span-to-depth ratio between 2.5 and 3.5 were governed by beam action, in which increasing the number of stirrups increased the shear capacity but decreased the angle of inclination. The strain of the longitudinal reinforcement in the beams with span-to-depth ratio of 2.5 and 3.5 was less than the strain in beams of span-to-depth ratio of 1.5, because the beams having a span-to-depth ratio of 2.5 and 3.5 relied less on the longitudinal reinforcement compared to the beams with a span-to-depth ratio of 1.5.

Nabipaylashgari (2012) also evaluated various design codes and guidelines (CSA-S806-12, CSA-S6-10, ACI 440-1R-06, and ACI 440-4R-04) and found that all codes and guidelines conservatively calculate the nominal shear capacity of the beams. Nabipaylashgari concluded that the concrete shear capacity formula used by ACI 440-4R-04 does not account the beneficial effects of prestressing in the shear capacity of prestressed concrete beams reinforced with FRP. Both CSA-S6-10 and CSA-S806-12 are less conservative then ACI 440-4R-04, with CSA-S806-12 being 12% less conservative than CSA-S6-10 because CSA-S806-12 takes into account the prestressing effects for concrete beams prestressed with FRP.

2.3 Performance of Carbon-Fiber-Reinforced Polymer Stirrups in Prestressed-Decked Bulb T-Beams

Grace et al. (2015) conducted an experiment in two phases. The first phase tested the effective bend and bending strength of Carbon Fiber Composite Cable (CFCC) stirrups, while the second phase tested 11 T-beams reinforced with steel and CFCC stirrups under one-point load. The beams had span-to-depth ratios of 3, 4, 5, and 6; prestressing levels of 0, 320, 444, 587 kN; and stirrup spacing of 102, 152, and 203 mm. Nine beams were prestressed with CFCC strands, and one beam was prestressed with steel strands. One beam was reinforced with non-prestressed CFCC strands. The cross section of the beams and the beam test setup are presented in Figures 2.4 and 2.5, respectively.

Figure 2.4. Cross Section of T-beams (Grace et al., 2015)

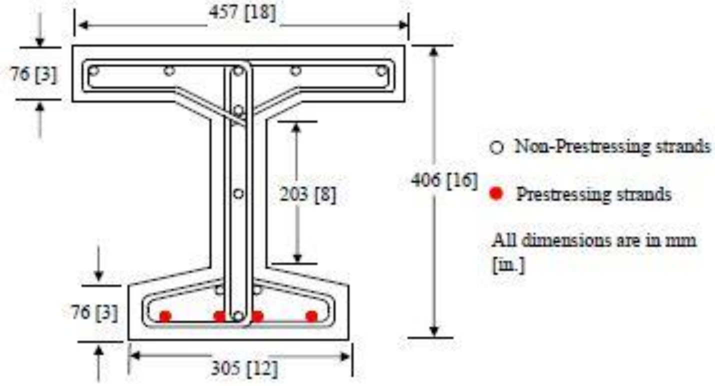

Figure 2.5. Beam test Setup (Grace et al., 2015)

The CFCC longitudinal reinforcement strands were 15.2 mm in diameter, with tensile stress of 2,930 MPa and modulus of elasticity of 149 GPa. The CFCC stirrups were 11.2 mm in diameter, with tensile stress of 2,840 MPa and modulus of elasticity of 150 GPa. The non-prestressed steel reinforcement strands were 15.2 mm in diameter, with yielding stress of 414 MPa and modulus of elasticity of 200 GPa, while the prestressed steel reinforcement strands were 15.2 mm in diameter, with yielding stress of 1,585 MPa and modulus of elasticity of 200 GPa. The steel stirrups were 10 mm in diameter, with yielding stress of 414 MPa and modulus of elasticity of 200 GPa.

The researchers compared their experimental results with various guidelines (ACI 440.1R-06, ACI 440.4R-04, and AASHTO 2012) and proposed modifications to increase prediction accuracy of the nominal shear capacity. They concluded that stirrup type does not affect the shear capacity of beams. When stirrup failed at a strain between 0.003 and 0.004, the primary parameters that caused the flexural-shear cracks were the level of prestressing and shear span-to-depth ratio. Because the guidelines' nominal shear capacity calculations were conservative compared to the experimental results, the researchers recommended that the ACI guidelines be revised and the AASHTO guidelines be modified to increase prediction accuracy of the shear capacity of the beams (Grace et al., 2015).

2.4 Shear Behavior of Concrete Beams Pre-Stressed with Carbon Fiber Reinforced Polymer Tendons

Wang et al. (2019) tested three groups of rectangular beams prestressed with CFRP tendons. The first group consisted of beams not reinforced with stirrups, the second group consisted of beams reinforced with stirrups and prestressing tendons were bounded, and the third group consisted of beams reinforced with stirrups and prestressing tendons were unbonded. This research tested the beams under varying stirrup ratio, tendon types, total area of tendons, shear span-to-depth ratio, and prestressing levels. In addition, the researchers conducted a finite element investigation to better understand the mechanical performance of crack formation and expansion and the process of structural breakage. A total of 23 beams were tested; beam cross section and configuration are presented in Figure 2.6.

Figure 2.6. (a) Beam Reinforcement Configuration; (b) Beam Cross Section (Wang et al., 2019)

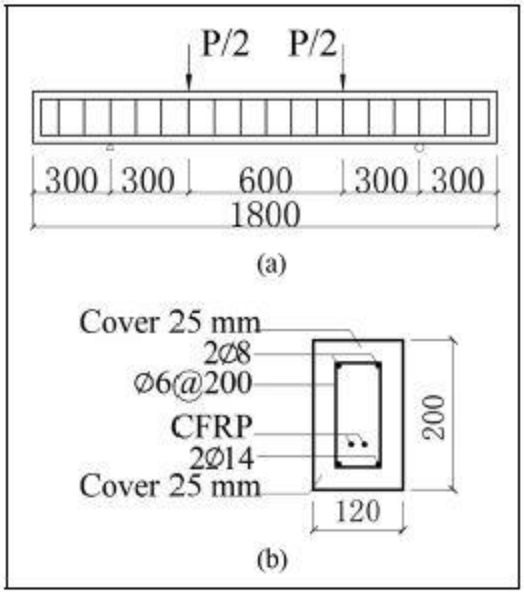

The materials used for longitudinal reinforcement were CFRP and steel. The CFRP reinforcements were 8 mm in diameter, 1,730 MPa in tensile strength, and 140 GPa in modulus, while the steel reinforcements were 9.5 mm in diameter, 1,766 MPa in tensile strength, and 195 GPa in modulus. The concrete was made in two batches, with an average compressive strength of 27.02 MPa for groups 1 and 2 and 36.80 MPa for group 3. The non-prestressed steel reinforcement and transverse reinforcement for groups 1 and 2 differed from group 3 because they were obtained from different manufacturers. Group 1 and group 2 used 14 mm diameter tension reinforcement with 268 MPa yield strength, and 200 GPa modulus; 8 mm diameter compression reinforcement with 331 MPa yield strength, and 200 GPa modulus; and 6 mm diameter stirrups with 309 MPa tensile strength, and 200 GPa modulus. Group 3 used 14 mm diameter tension reinforcement with 471 MPa yield strength, and 200 GPa modulus; 8 mm diameter compression reinforcement with 382 MPa yield strength, and 200 GPa modulus; and 6 mm diameter stirrups with 488 MPa tensile strength, and 200 GPa modulus.

The researchers concluded that stirrup ratio and shear span-to-depth ratio were the primary parameters that affect the shear capacity for prestressed concrete beams with CFRP tendons. The shear span-to-depth ratio was the parameter to determine the failure mode in beams. For beams without stirrups, the beams failed in compression of concrete when the shear span-to-depth ratio was lower than 1. Beams failed in shear compression when the ratio was between 1 and 2.5, and they failed in flexure when the ratio was higher than 2.5. For beams with stirrups, when the span-to-depth ratio was lower than 1.3, the beams failed in compression of concrete; when the ratio was between 1.3 and 2.6, the beams failed in shear compression, and when the ratio was higher than 2.6, the beams failed in flexure (Wang et al., 2019).

2.5 General Summary

Overall, the literature showed that the prestressing level, stirrup ratio, and shear span-to-depth ratio are factors that affect the shear capacity of prestressed beams reinforced with CFRP. Grace et al. (2015) showed that, as the prestressing level increased from 0, to 72, 100, and 132 kips, the maximum shear capacity increased from 9.5, to 23.5, 27.8, and 30.3 kips, respectively. If the stirrup ratio is very high due to increased total stirrup area, decreased stirrup spacing, or both, the beams could fail prematurely, as demonstrated with a stirrup spacing of 4 inches. Park and Naaman (1999), Wang et al. (2019), and Grace et al. (2015) all showed that beam shear capacity increases when the stirrup ratio increases. If the stirrup ratio is low, however, shear cracking between the stirrups causes the beams to fail and the shear capacity to decrease.

Previous study results also showed that arch action causes beams to fail in compression of concrete when the shear span-to-depth ratio is lower than 1.5; when the ratio exceeds 1.5, the beams fail in tension or compression shear crack due to beam action. However, for shear span-to-depth ratio larger than 2.5, the beam cross section and stirrups ratio governed the mode of failure between flexural or shear failure. For example, Wang et al. (2019) showed that beams with a span-to-depth ratio higher than 2.6 failed in flexural, whereas Grace et al. (2015) showed that beams with a shear span-to-depth ratio larger than 3 failed in shear.

Yet more experimental studies with diverse parameters are required to improve and solidify the conclusions made for prestressed concrete beams reinforced with CFRP tendons. Due to the lack of experimental studies with varied parameters, the design guidelines for calculating the nominal shear capacity of prestressed concrete beams reinforced with CFRP tendons published by different institutions such as ACI and AASHTO are largely conservative. Thus, to improve and transform these current shear design guidelines to shear design codes more experimental studies with diverse parameters are required.

Chapter 3 – Shear Design Guidelines for Prestressed Concrete Beams Reinforced with CFRP

This chapter introduces shear design guidelines for prestressed concrete beams reinforced with CFRP tendons. Those guidelines include *Prestressing Concrete Structures with FRP Tendons* (ACI 440.4R-04, 2004) and *Design of Concrete Bridge Beams Prestressed with Carbon Fiber-Reinforced Polymer (CFRP) Systems* (AASHTO, 2018). A comparison between ACI 440.4R-04 and AASHTO 2018 is included at the end of the chapter.

3.1 Truss Model and Corresponding Design Approaches

This section introduces the 45° truss model, including its inception and evolution, as well as how ACI 440.4R-04 modified it for shear design.

3.1.1 The 45° Truss Model

In 1899, Ritter introduced the 45° truss model to reinforced concrete beams with stirrups as vertical tension members and diagonal concrete stresses as diagonal compression members. Longitudinal reinforcement was the tension cord, and concrete compression area was the compression cord, as illustrated in Figure 3.1.

Figure 3.1. Ritter's Truss Analogy for Shear

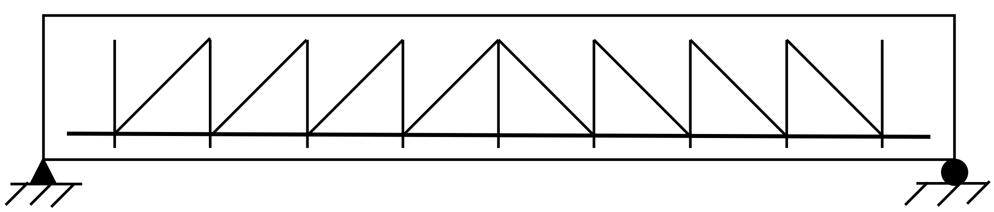

In 1902, Mörsch added to Ritter's work by demonstrating that concrete compression diagonal members did not have to reach the top of one stirrup and the bottom of the adjacent stirrup. Mörsch's work also showed that diagonal concrete stresses were a continuous field of compression stresses rather than a single stress between stirrups (Figure 3.2).

Figure 3.2. Mörsch's Truss Model (Collins & Mitchell, 1997)

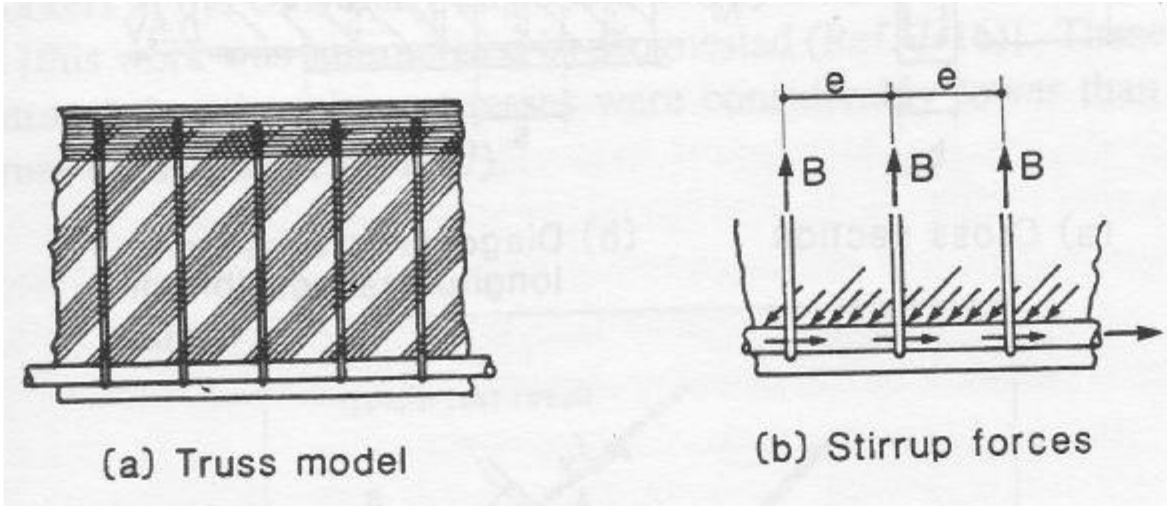

Therefore, neglecting the tension component of the cracked concrete and assuming that the diagonal compression stresses are at 45° angles, the concrete principle compressive stress and the stirrup stresses can be calculated using a free-body diagram, as shown in Figure 3.3.

Figure 3.3. Equilibrium Considerations for 45◦ Truss Model (Collins & Mitchell, 1997)

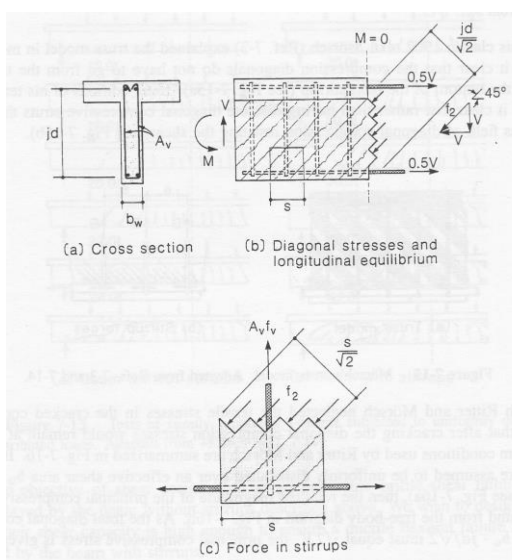

To calculate the principle compressive stress, the shear stresses must be assumed to be uniformly distributed over $b_w$wide and jd deep as illustrated in Figure 3.3-a. Thus, the principle concrete compressive stress, f_2, from Figure 3.3-b is as follows:

$$\sqrt{2}V = \frac{f_2 b_w jd}{\sqrt{2}} \tag{1}$$

$$f_2 = \frac{2V}{b_w jd} \tag{2}$$

Summing the vertical forces in Figure 3.3-b reveals the tensile force in the longitudinal reinforcement, N_v, due to the shear force:

$$N_v = V \tag{3}$$

Finally, summing the forces in the *y*-axis in Figure 3.3-c reveals the tensile force in the stirrup:

$$\frac{V}{jd} = \frac{f_v A_v}{S}, \tag{4}$$

where f_v is the stirrup's tensile stress, S is the stirrup spacing, and A_v is the cross-sectional area of the stirrup's legs.

3.1.2 ACI 440.4R-04

According to ACI 440.4R-04 that is based on ACI 318-02, for beams with FRP shear reinforcement, the nominal shear strength of concrete, V_n, is the sum of the shear resistance provided by concrete, V_c, the shear resistance provided by stirrups made from FRP, V_{frp}, and the shear resistance provided by the vertical component of prestressing force, V_p:

$$V_n = V_c + V_{frp} + V_p, \tag{5}$$

where V_{frp}, similar to equation (4), is equal to

$$V_{frp} = \frac{f_{fb} A_v d}{S}, \tag{6}$$

and where A_v is the total cross-sectional area of the stirrups, d is the effective depth, S is the stirrup spacing, and f_{fb} is calculated as

$$f_{fb} = \phi_{bend} f_{fu} \leq 0.002 E_{s,frp} \tag{7}$$

The ϕ_{bend} value was modified from JSCE (1997) and calculated as

$$0.25 \leq \phi_{bend} = 0.11 + 0.05 \frac{r}{d_b} \leq 1.0, \tag{8}$$

where r is the radius of the bend, d_b is the diameter of the reinforcing bar, f_{fu} is the ultimate tensile strength of the FRP stirrup, and $E_{s,frp}$ is the modulus of elasticity of the stirrup. V_c was calculated as follows:

$$V_c = 2\sqrt{f'_c} b_w d \text{ (lb)} \tag{9}$$

where $f'c$ is the concrete compressive strength (psi), b_w is the effective width (in.), and d is the effective depth of the section from the top fibers to the center of the longitudinal reinforcement (in.).

The maximum spacing of shear reinforcement for prestressed members was limited to $0.75h$, or 24 inches, to prevent large crack width. The maximum stirrup spacing was reduced by half when the maximum shear V_{frp} exceeded $4.0\sqrt{f'_c} b_w d$ (lb). These limits ensured small and uniformly distributed shear cracks along the beam.

To prevent sudden formation of large cracks that could result in shear failure in the beam, a minimum amount of shear reinforcement was required when V_u, the factored shear force at a section, exceeded $\frac{\phi V_c}{2}$. $A_{v,min}$ was calculated using the following equation:

$$A_{v,min} = 0.75\sqrt{f'_c} \frac{b_w S}{\phi_{bend} f_{fu}} \text{ (lb)} \tag{10}$$

3.2 Compression Field Theory and Corresponding Design Approaches

This section introduces the compression field theory (CFT), the modified compression field theory (MCFT), and the simplified modified compression field theory (SMCFT). Detailed explanation is also provided as to how AASHTO 2018 modified SMCFT for shear design.

3.2.1 Compression Field Theory

Compression Field Theory (CFT) is the inverse of the tension field theory developed by Wagner in 1929 (Wight, 2016). Wagner used the tension field theory to study the post-buckling shear resistance of thin-webbed metal girders. Wagner's theory assumed that, after buckling, the thin webs would not resist compression and the diagonal tension field would resist shear, as shown in Figure 3.4.

Figure 3.4. Tension Field in Thin-Webbed Metal Girder with Shear (Collins & Mitchell, 1997)

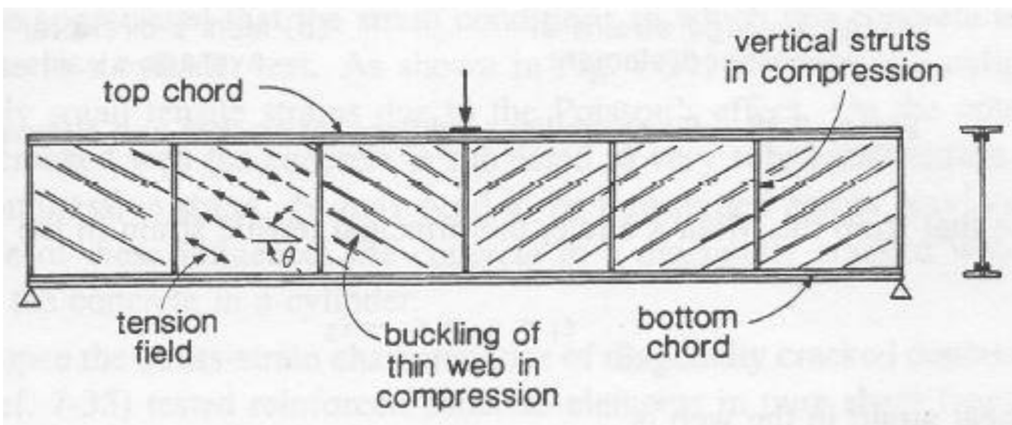

Thus, by inverting the tension field theory for reinforced concrete, where the shear is resisted by the diagonal compression field instead of the diagonal tension field, the angle of inclination was calculated using the average strains in the cracked element shown in figure 3.5(a).

$$tan^2(\theta) = \frac{\epsilon_x - \epsilon_2}{\epsilon_t - \epsilon_2}, \tag{11}$$

where ϵ_x is the longitudinal strain in the web ([+] if tension), ϵ_t is transverse strain ([+] if tension), and $\epsilon_2$is the principle compressive strain ([-] if tension).

Using Mohr's Circle, shown in Figure 3.5(b), for a given θ, both the principal tensile strain and shear strain in the web were calculated using equations (12) and (13), respectively.

Figure 3.5. Compatibility Condition for Cracked Web Element (Collins & Mitchell, 1997)

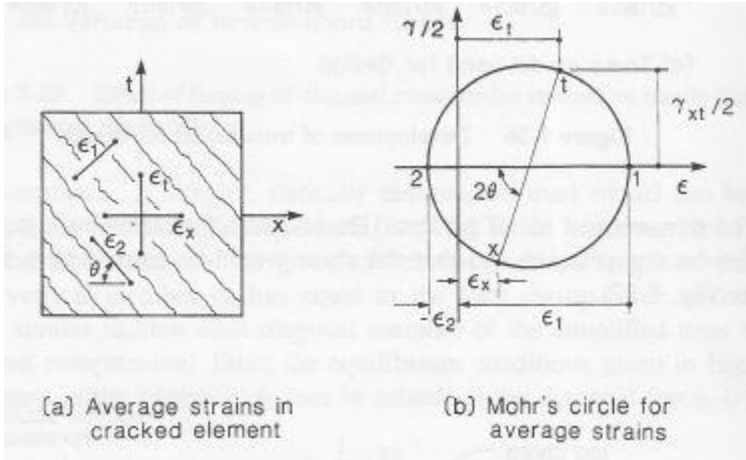

$$\epsilon_1 = \epsilon_x + \epsilon_t - \epsilon_2 \tag{12}$$

$$\gamma_{xt} = 2(\epsilon_x - \epsilon_2)\cot(\theta) \tag{13}$$

Five unknowns (f_x, longitudinal bar stress; f_v, stirrups stress; f_p, longitudinal prestressing stress; f_2, diagonal concrete compressive stress; and θ, angle of inclination) had to be determined in order to calculate the shear, V, in a symmetrically reinforced, longitudinally prestressed concrete beam. The unknowns were calculated using equilibrium, stress-strain relationships, and compatibility, as summarized in Figure 3.6.

Figure 3.6. CFT for Prestressed Beam Subjected to Shear (Collins & Mitchell, 1997)

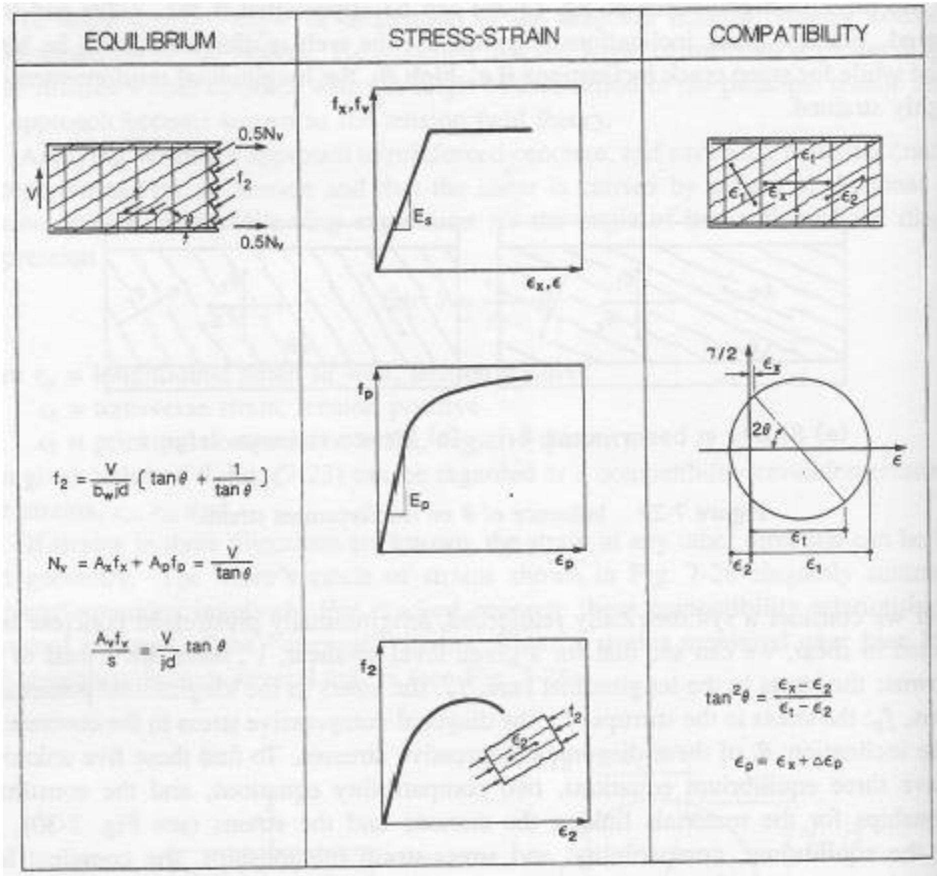

One disadvantage of the CFT is that it overestimates deformations and offers conservative shear strength because it neglects tensile stress contribution to the cracked concrete. MCFT rectifies this fault by including the contribution of the tensile stress.

3.2.2 Modified Compression Field Theory

Although the principle tensile is assumed to be zero in the CFT, the MCFT accounts for the principle tensile stress, f_1, between concrete cracks. Using a symmetrical cross section in pure shear, as shown in Figure 3.7, equilibrium conditions for the MCFT were created. However, because tensile stresses in diagonally cracked concrete vary in magnitude, the tensile stresses were taken as the average value when formulating the equilibrium equations (Collins & Mitchell, 1997).

Figure 3.7. Equilibrium Conditions of MCFT (Collins & Mitchell, 1997)

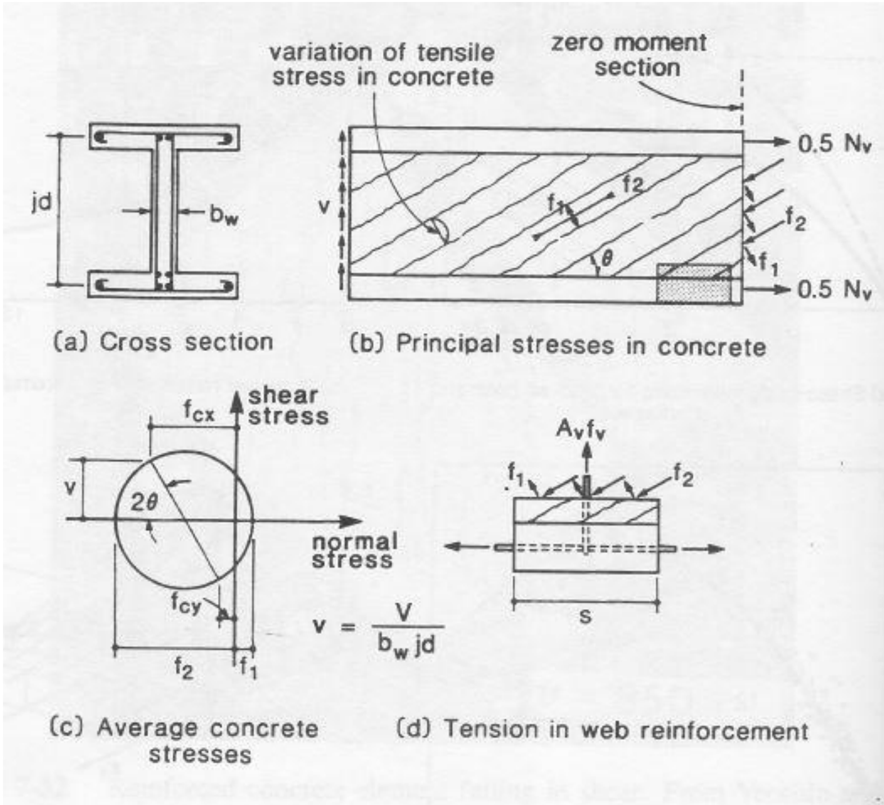

Using Mohr's circle (Figure 3.7), the principle compressive stresses, f_2, can be expressed as follows:

$$f_2 = [\tan(\theta) + \cot(\theta)]\, v - f_1, \tag{14}$$

where v is equal to

$$v = \frac{V}{b_w jd} \tag{15}$$

Since diagonal compression stresses push apart the flanges of the beam and diagonal tensile stresses pull the flanges together, web reinforcement must be used to resist the resulting imbalance, as shown in Figure 3.7(d), resulting in

$$A_v f_v = (f_2\, sin^2(\theta) - f_1\, cos^2(\theta))\, b_w s, \tag{16}$$

where f_v is the average stress in the stirrups. Substituting f_2 and v in equation (16) results in

$$V = f_1 b_w jd \cot(\theta) + \frac{f_v A_v jd}{S} \cot(\theta), \tag{17}$$

where V is the additive shear resistance of the member, the first part on the right-hand side of equation (17) is the concrete shear resistance, and the second part of equation (17) is the steel shear resistance.

If the axial load on the beam is equal to zero, then a new equilibrium expression can be expressed by equalizing the unbalanced longitudinal component of the diagonal concrete stress to the tensile stresses in the flexural reinforcement:

$$A_{sx} f_l + A_{px} f_p = (f_2 \, cos^2(\theta) - f_1 \, sin^2(\theta)) \, b_w jd, \tag{18}$$

where A_{sx} is the total area of the non-prestressed reinforcement, A_{px} is the total area of the prestressed reinforcement, f_l is the average stress of the non-prestressed flexural reinforcement, and f_p is the average stress of the prestressed flexural reinforcement. Substituting f_2 in equation (18) results in

$$A_{sx} f_l + A_{px} f_p = V \cot(\theta) - f_1 b_w jd \tag{19}$$

Notably, the equations (17) to (19) do not account for local variation in a concrete crack section. For example, the tensile stresses of concrete in a crack section reaches zero, while tensile stresses in reinforcement increase, as shown in Figure 3.8. The shear capacity of the member is limited by the ability of the member to transmit forces across the crack (Collins & Mitchell, 1997).

Figure 3.8. Transmitting Forces Across Cracks (Vecchio & Collins, 1986)

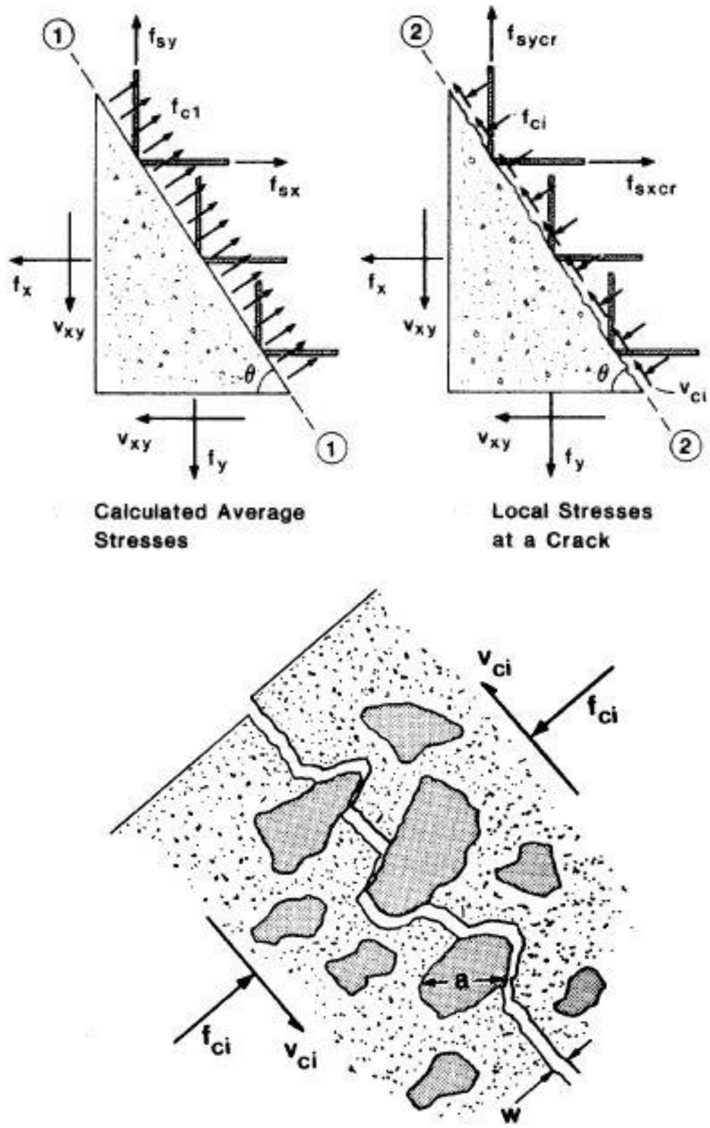

The local shear stress, v_{ci}, is limited by equation (20) and dependent on the crack width, which can be calculated using equation (21):

$$v_{ci} = \frac{2.16\sqrt{f'_c}}{0.3 + \frac{24w}{a + 0.63}} \tag{20}$$

$$w = \epsilon_1 s_{m\theta}, \tag{21}$$

where a is the maximum aggregate size, $\epsilon_1$is the principle tensile strain, and $s_{m\theta}$ is the average spacing of the diagonal crack, calculated by

$$s_{m\theta} = \frac{1}{\frac{\sin(\theta)}{s_{mx}} + \frac{\cos(\theta)}{s_{mv}}} \tag{22}$$

where s_{mx} and s_{mv} are the crack spacing, indicative of crack-control characteristics of longitudinal and transverse reinforcement respectively, as shown in Figure 3.9.

Figure 3.9. Spacing of Inclined Cracks (Collins & Mitchell, 1997)

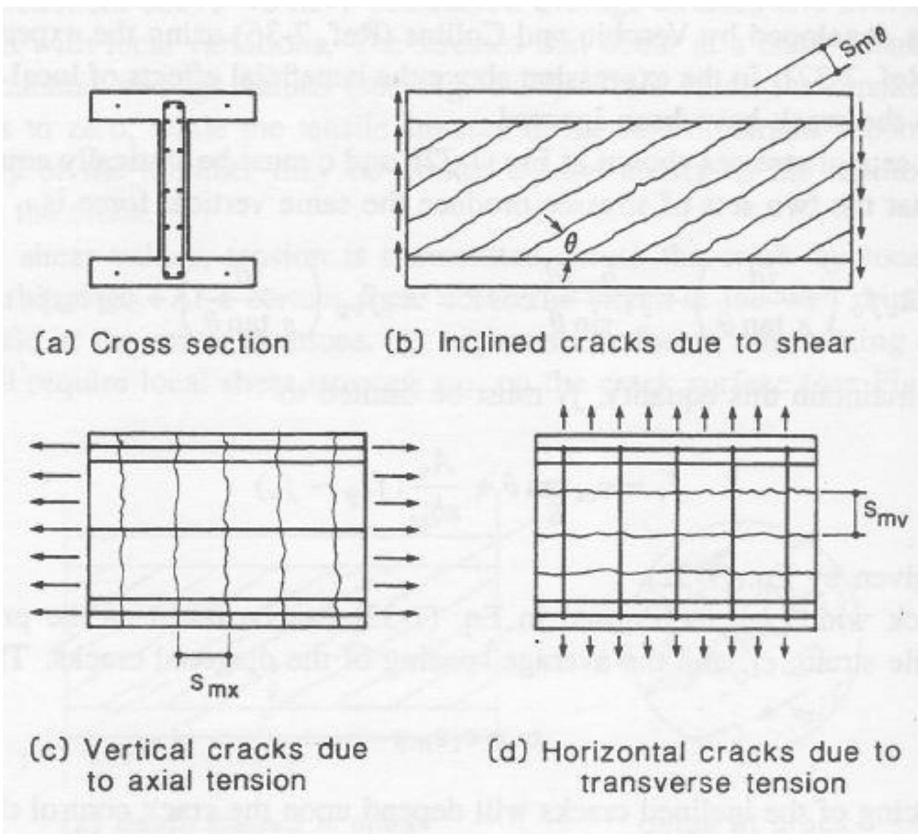

Since average stresses and local stresses are statically equivalent (Figure 3.8), they produce the same vertical force, as shown in the following equilibrium equation:

$$A_v f_v \left(\frac{jd}{S\tan(\theta)}\right) + f_1 \frac{b_w jd}{\sin(\theta)} \cos(\theta) = A_v f_{vy} \left(\frac{jd}{S\tan(\theta)}\right) + v_{ci} b_w jd, \tag{23}$$

Therefore, f_1 must be limited to $\frac{A_v}{b_w S}\left(f_{vy} - f_v\right) + v_{ci}\tan(\theta)$ to maintain equality in equation (23).

3.2.3 Simplified Modified Compression Field Theory

Bentz et al. (2006) used results of over 100 tests of reinforced concrete under pure shear to develop the Simplified Modified Compression Field Theory (SMCFT). The objective of their research was to find a simpler method to predict shear strength of reinforced concrete than the MFCT, which requires many steps and multiple iterations. SMCFT derivation began with the MCFT equation, as shown in Figure 3.10.

Figure 3.10. MCFT Equations (Bentz et al., 2006)

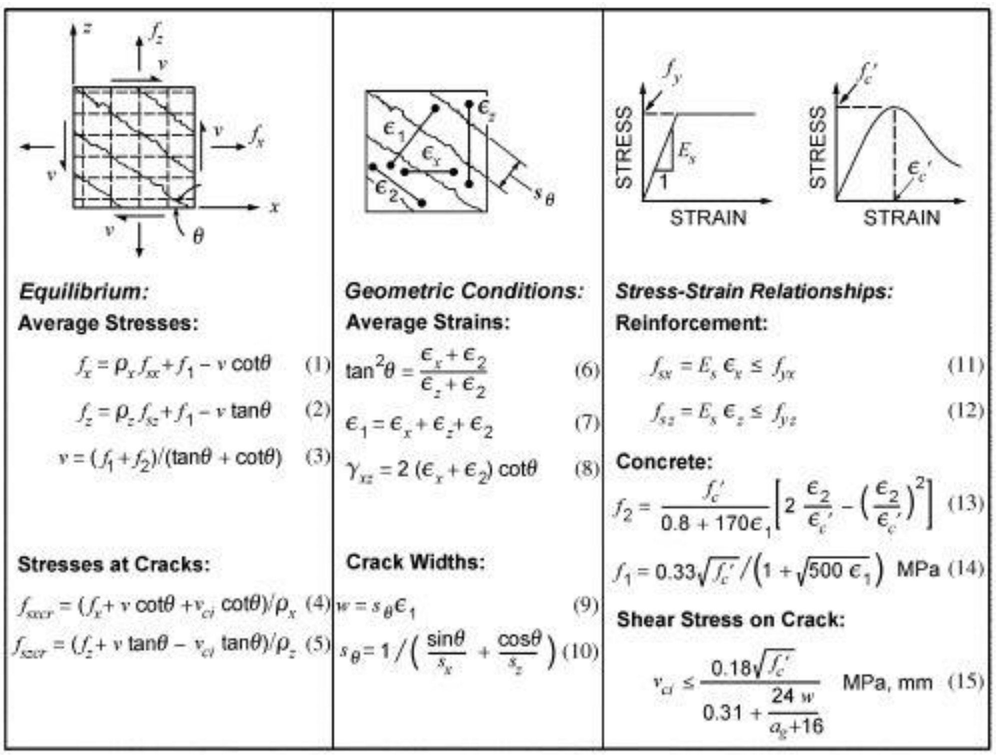

Assumptions, such as clamping stress f_z is negligibly small, were then made. For failures occurring before stirrup yielding, the failure shear stress was $0.25f'_c$, while the failure of f_{sz} and f_{szcr} were equal to yielding stress f_y of the stirrups for failures occurring below the shear stress.

Summing the forces in the *z*-direction using the assumptions above and the free-body diagram (Figure 3.11), the shear stress was equal to

$$v = v_c + v_s = \beta\sqrt{f'_c} + \rho_z f_y \cot(\theta), \tag{24}$$

where β for beams without transverse reinforcement is the function of the longitudinal strain, ε_x, and the crack spacing, s_{xe}, and can be calculated by

$$\beta = \frac{4.8}{1 + 1500\varepsilon_x} * \frac{51}{39 + s_{xe}}, \tag{25}$$

where s_{xe} is

$$s_{xe} = \frac{1.38 s_x}{a_g + 0.63} \tag{26}$$

where a_g is the maximum coarse aggregate size and s_x is the vertical distance between bars aligned in the *x*-direction.

Figure 3.11. Transmission of Forces Across Cracks (Bentz et al., 2006)

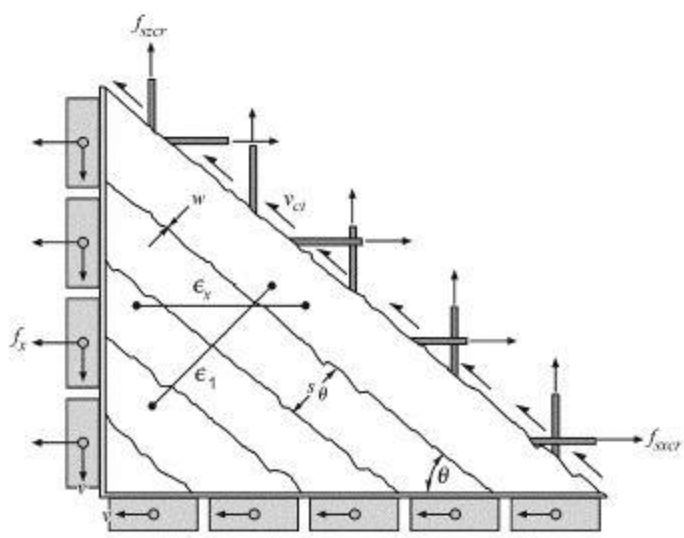

The angle of inclination, θ, was assumed to be the function of both ε_x and s_{xe}:

$$\theta = (29deg + 7000\varepsilon_x) * \left(0.88 + \frac{s_{xe}}{100}\right) \leq 75deg \tag{27}$$

Since reinforced concrete beams are reinforced with transverse reinforcement, the magnitude between v_s and v_c was very different. Due to yielding of the transverse reinforcement, the value of v_s increased as the value of θ became smaller, while $\varepsilon_1$increased, causing v_c to decrease. In reinforced concrete beams with sufficient transverse reinforcement, crack spacings are typically less than a conservative 12 inches. Thus, the effect of the cracked concrete width can be neglected simplifying equations (25) and (27) to

$$\beta = \frac{4.8}{1 + 1500\varepsilon_x} \tag{28}$$

$$\theta = (29deg + 7000\varepsilon_x) \leq 75deg \tag{29}$$

Comparison results of equations (28) and (29) to the MCFT's β and θ showed that the equations were conservative over the range of 0.5×10^{-3} to 2.0×10^{-3} of ε_x. However, when ε_x was less than 0.5×10^{-3}, β was not conservative while θ remained conservative (Figure 3.12).

Figure 3.12. SMCFT Values for Theta and Beta with Transverse Reinforcement (Bentz et al., 2006)

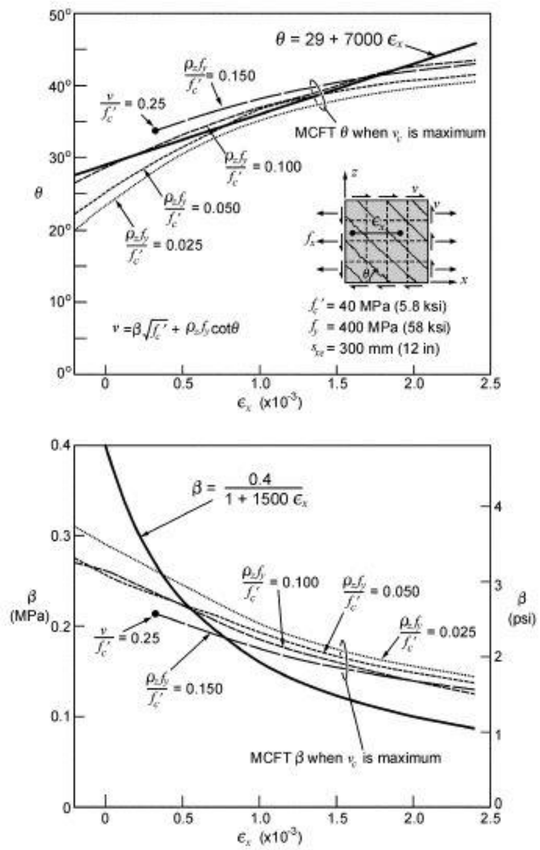

3.2.4 AASHTO 2018

According to AASHTO LRFD (2014) general procedure, the nominal shear strength, V_n, is equal to the lesser of

$$V_n = V_c + V_f + V_p \tag{30}$$

$$V_n = 0.2f'_c b_v d_v + V_p, \tag{31}$$

where the concrete shear strength, V_c, is displayed as

$$V_c = 0.0316\beta\sqrt{f'_c} b_v d_v \text{ (kips)}, \tag{32}$$

and the transverse reinforcement shear strength, V_f, is displayed as

$$V_f = \frac{A_v f_f d_v (cot\theta + \cot\alpha) * \sin(\alpha)}{S} \text{ (kips)}, \tag{33}$$

where b_v is the effective web width taken as the minimum width within d_v; d_v is the effective depth equal to the larger of $0.9d_e$, $0.72h$, or $\frac{M_n}{A_{pf} f_{pf} + A_f f_f}$; S is the transverse reinforcement spacing; θ is the angle of inclination; α is the angle of transverse reinforcement inclination; A_v is the area of transverse reinforcement; V_p is the vertical component of the effective prestressed force; h is the total depth of the beam; d_e is equal to $\frac{A_{pf} f_{pf} d_p + A_f f_f d_f}{A_{pf} f_{pf} + A_f f_f}$; f_f is the transverse reinforcement corresponding to strain of 0.0035; A_{pf} is the area of prestressed reinforcement on the flexural tension area; and A_f is the area of non-prestressed reinforcement on the flexural tension area.

The procedure to determine β and θ is as follows:

If $A_v \geq A_{v,min}$, then

$$\beta = \frac{4.8}{1 + 750\varepsilon_f} \tag{34}$$

If longitudinal strain (ε_f) is positive (i.e., the section is in tension), then

$$\varepsilon_f = \frac{\frac{|M_u|}{d_v} + 0.5N_u + \left|V_u - V_p\right| - A_{pf} f_{po}}{E_f A_f + E_p A_{pf}} \tag{35}$$

However, if longitudinal strain (ε_f) is negative (i.e., the section is under compression), then ε_f can be conservatively equal to zero or calculated as

$$\varepsilon_f = \frac{\frac{|M_u|}{d_v} + 0.5N_u + \left|V_u - V_p\right| - A_{pf} f_{po}}{E_f A_f + E_p A_{pf} + E_c A_c} \tag{36}$$

where M_u is the factored moment load that is more than $\left|V_u - V_p\right| d_v$; V_u is the factored shear load; N_u is the factored axial load that is positive if tensile but negative if compressive; A_c is the area of concrete on the flexural tension side of the section; and f_{po} is a parameter taken as the modulus of elasticity of the prestressing tendons multiplied by the locked-in difference in strain between the prestressing tendons and the concrete. For usual prestressing levels, the value of $0.6f_{pu}$ is appropriate.

If $A_v < A_{v,min}$, then

$$\beta = \frac{4.8}{1 + 750\varepsilon_f} \times \frac{51}{39 + s_{xe}}, \tag{37}$$

where the crack spacing, s_{xe}, is

$$s_{xe} = \frac{1.38s_x}{a_g + 0.63}, \tag{38}$$

and a_g is the maximum aggregate size.

The area of the transverse reinforcement, A_v, must be larger than the minimum transverse reinforcement, $A_{v,min}$, where $A_{v,min}$ is

$$A_{v,min} = 0.0316\sqrt{f'_c}\frac{b_v S}{f_f} \tag{39}$$

Similarly, spacing of the transverse reinforcement must not exceed the maximum spacing, S_{max}, determined as follows:

If $v_u < 0.125f'_c$

$$s_{max} = 0.8d_v \leq 24in \tag{40}$$

If $v_u \geq 0.125f'_c$

$$s_{max} = 0.4d_v \leq 12in, \tag{41}$$

where v_u is the shear stress equal to $\frac{|V_u - \emptyset V_p|}{\emptyset b_v d_v}$ and $\emptyset = 0.75$.

3.3 Comparison of ACI 440.4R-04 and AASHTO 2018

A comparison of the ACI 440.4R-04 and AASHTO 2018 guidelines showed that nominal shear strength is the sum of the concrete shear strength, the transverse shear reinforcement strength, and the vertical component of the prestressing force. Although the models to calculate concrete shear strength and transverse shear reinforcement strength are similar, one minor difference is that the effective depth in ACI 440.4R-04, d, is depth from the concrete top fiber to the centroid of the prestressing tendon, whereas in AASHTO 2018, d_v is the effective depth equal to the largest of $0.9d_e$, $0.72h$, or $\frac{M_n}{A_{pf}f_{pf}+A_f f_f}$. Stress of the transverse reinforcement for ACI 440.4R-04 is calculated using equation (7), while stress of the transverse reinforcement in AASHTO 2018 is equal to $0.0035E_s$.

Differences between the two guidelines are primarily due to their unique foundational theories. ACI 440.4R-04 is based on the 45° truss model, which assumes that the angle of inclination, Θ, is equal to 45°. However, this assumption neglects shear resistance from the longitudinal reinforcement, resulting in significantly conservative results. On the other hand, AASHTO 2018 is based on the SMCFT, which considers the effects of longitudinal reinforcement by calculating strain of the longitudinal reinforcement, ε_f. As the ε_f increases, the Θ increases, resulting in a decreased transverse shear reinforcement strength, and as the ε_f decreases, the Θ decreases, resulting in an increased transverse shear reinforcement strength.

The guidelines also differ in their values of β. At the time of ACI 440.4R-04 publication, sufficient studies on shear behavior for prestressed concrete beams reinforced with FRP were lacking, so that the committee selected the minimum β (equal to 2) according to ACI 318-02. The β value in AASHTO 2018 varies, however, depending on the ε_f and the amount of transverse reinforcement. Overall, the procedure detailed in ACI 440.4R-04 is more user-friendly since all parameters are known and the user input is minimal. In contrast, AASHTO 2018 requires more user input because it includes the effect of the longitudinal reinforcement from both parameters V_u and M_u, which change along the beam and require the analysis location to accurately calculate V_n.

Chapter 4 – Evaluating Design Guides with Experimental Data

This study used the concrete beams listed in Table 4.1 which were from previous experimental studies (Grace et al., Park and Naaman, Wang et al., and Nabipaylashgari) to evaluate ACI 440.4R and AASHTO 2018 shear strength design guidelines. All the specimens were concrete beams pretension with CFRP tendons and reinforced with steel or FRP stirrups. The specimens all failed in shear.

Table 4.1. Specimens Selected

Reference	#	Specimens
Grace et al., 2015	1	C100-C6-3
	2	C100-C6-4
	3	C100-C6-5
	4	C100-C6-6
	5	C100-S6-3
	6	C100-S6-4
	7	C100-S6-5
	8	C100-S6-6
	9	C100-C4-3
	10	C100-C8-3
	11	C100-S4-3
	12	C100-S8-3
	13	C072-C4-3
	14	C132-C4-3
	15	C072-S4-3
	16	C132-S4-3
Park and Naaman, 1999	17	C5
	18	C7
	19	C9
	20	C10
Wang et al., 2019	21	PCII-3
	22	PCII-4
	23	PCII-5
	24	PCII-6
Nabipaylashgari, 2012	25	PR-1.5-S
	26	PR-2.5-S
	27	PR-2.5-S
	28	PR-3.5-S
	29	PR-3.5-S

Evaluation of the guidelines included a comparison of the beams' nominal shear capacity (V_n) to the experimental shear capacity (V_{exp}), followed by an examination of the effects of the stirrup ratio ($^{A_v}/_{S}$), shear span-to-depth ratio ($^{a}/_{d}$), and longitudinal prestressed reinforcement effect on the angle of inclination (Θ) and β.

4.1 ACI 440.4R-04

This study used ACI 440.4R to calculate the V_n and compare it to V_{exp}, as described in Section 3.1.2. The ratio of this comparison, $^{V_{exp}}/_{V_n}$, produced a conservative result (Figure 4.1) due to the 45° truss model used by ACI 440.4R to calculate V_n.

Figure 4.1. V_{exp}/V_n Ratio (ACI 440.4R)

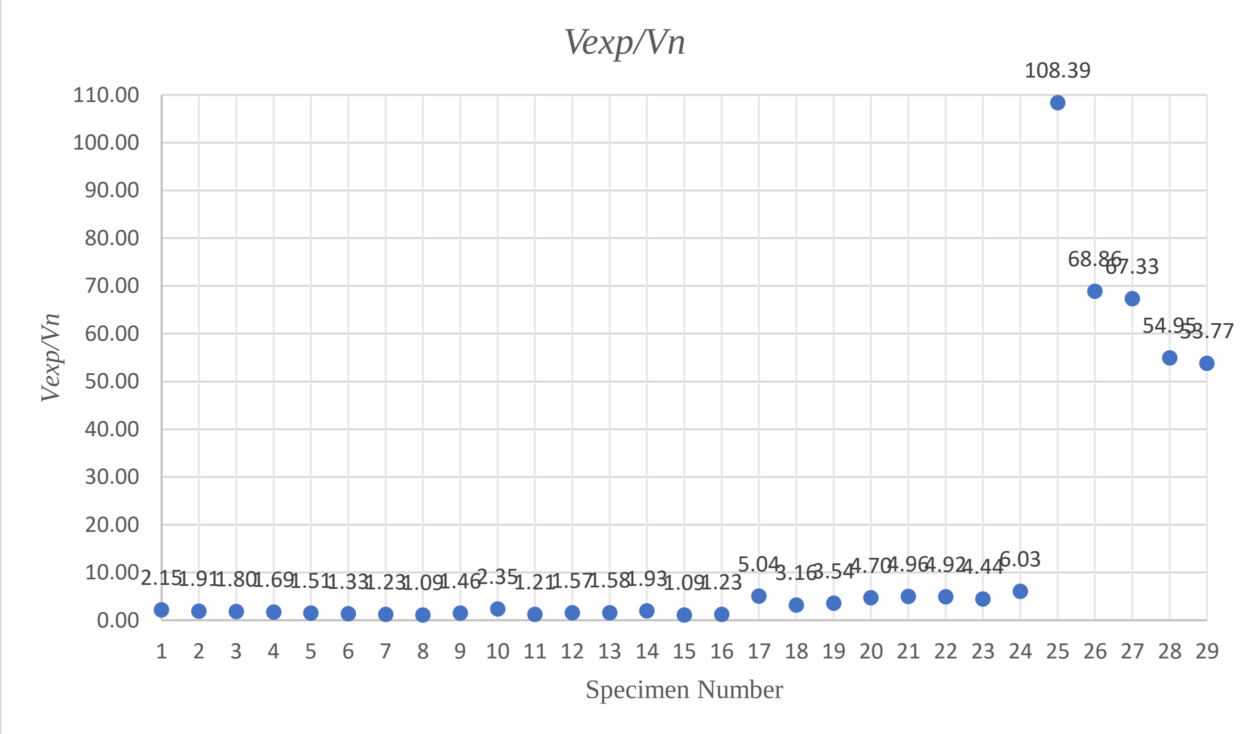

As shown in Figure 4.1, the average $^{V_{exp}}/_{V_n}$ ratio was 14.32, with a maximum ratio of 108.4 and a minimum ratio of 1.09. The discrepancy between the nominal and experimental results is primarily attributed to the neglect of the prestressed longitudinal reinforcement strain effect on both Θ and β. As discussed in Section 3.1.1, ACI 440.4R uses the 45° truss model to calculate V_n. This model assumes Θ to be 45°, where the experimental angle of inclination, θ_{exp}, is less than 45°, as shown Table 4.2.

Table 4.2. θ_{exp} Form of the Selected Specimens

#	Specimens	Θ_{exp} (degree)
1	C100-C6-3	33-37
2	C100-C6-4	27-46
3	C100-C6-5	35-45
4	C100-C6-6	32-44
5	C100-S6-3	32-36
6	C100-S6-4	31-36
7	C100-S6-5	38-47
8	C100-S6-6	29-44
9	C100-C4-3	32-45
10	C100-C8-3	31-32
11	C100-S4-3	29-38
12	C100-S8-3	28-36
13	C072-C4-3	37-39
14	C132-C4-3	37-43
15	C072-S4-3	28-38
16	C132-S4-3	28-39
17	C5	-
18	C7	-
19	C9	-
20	C10	-
21	PCII-3	-
22	PCII-4	-
23	PCII-5	-
24	PCII-6	-
25	PR-1.5-S	43
26	PR-2.5-S	30,44
27	PR-2.5-S	32,44
28	PR-3.5-S	19,31,36,45
29	PR-3.5-S	22,30,41

Typically, when strain in the longitudinal reinforcement decreases, Θ decreases, thereby increasing the transverse shear capacity, V_f, and V_n. Conversely, when strain in the longitudinal reinforcement increases, Θ increases, thereby decreasing the transverse shear capacity, V_f, and

V_n. By assuming that Θ was equal to 45°, the beams with Θ_{exp} close to or equal to 45°, such as specimen numbers 7, 8, and 9, had a V_{exp}/V_n ratio close to 1. However, for beams with Θ_{exp} less than 45°, such as specimen numbers 1, 2, and 29, the V_{exp}/V_n ratio was high. In addition, ACI 440.4R neglects the prestressing level. For example, when computing V_n for specimen numbers 13 and 14, where specimen 13 had a prestressing force of 72 kips and specimen 14 had a prestressing force of 132 kips, V_n was the same and equal to 36.8 kips. Disregarding the prestressing level effect on the shear capacity neglects the fact that shear capacity increases as the prestressing level increases (Figure 4.1) and the experimental result from Grace et al. (2015), where V_{exp} for C072-C4-3 and C132-C4-3 were 58.2 kips and 71.2 kips, respectively. In the case of β, ACI 440.4R utilizes the minimum limit value (i.e., 2) for β due to the limited research on shear behavior of prestressed concrete beams reinforced with CFRP at the time the report was published in 2004. However, making β equal to 2 neglects the effect that longitudinal reinforcement has on β since β and therefore V_c decrease as longitudinal strain increases. In contrast, as longitudinal strain decreases, β and V_c increase. Thus, using the minimum limit for β means the calculated V_c always results in the minimum conservative values for the concrete shear capacity, making V_n a more conservative result compared to V_{exp}, as shown in Figure 4.1.

ACI 440.4R also ignores the shear span-to-depth ratio a/d, a crucial parameter that affects shear capacity of the beam. The consequence of ignoring the a/d ratio was proven by calculating V_n for specimens 1–4, where the a/d ratio was 3, 4, 5, and 6, respectively, with the same calculated nominal shear capacity of 27.5 kips. Similarly, in specimens 26–29, where the a/d ratio was 2.5 for specimens 26 and 27 and 3.5 for specimens 28 and 29, the calculated nominal shear capacity was 1.32 kips. However, comparison results of the $^{a}/_{d}$ ratio to $^{V_{exp}}/_{V_n}$ revealed an interesting pattern (Figure 4.2).

Figure 4.2. Comparison of *a/d* Ratio and V_{exp}/V_n (ACI 440.4R)

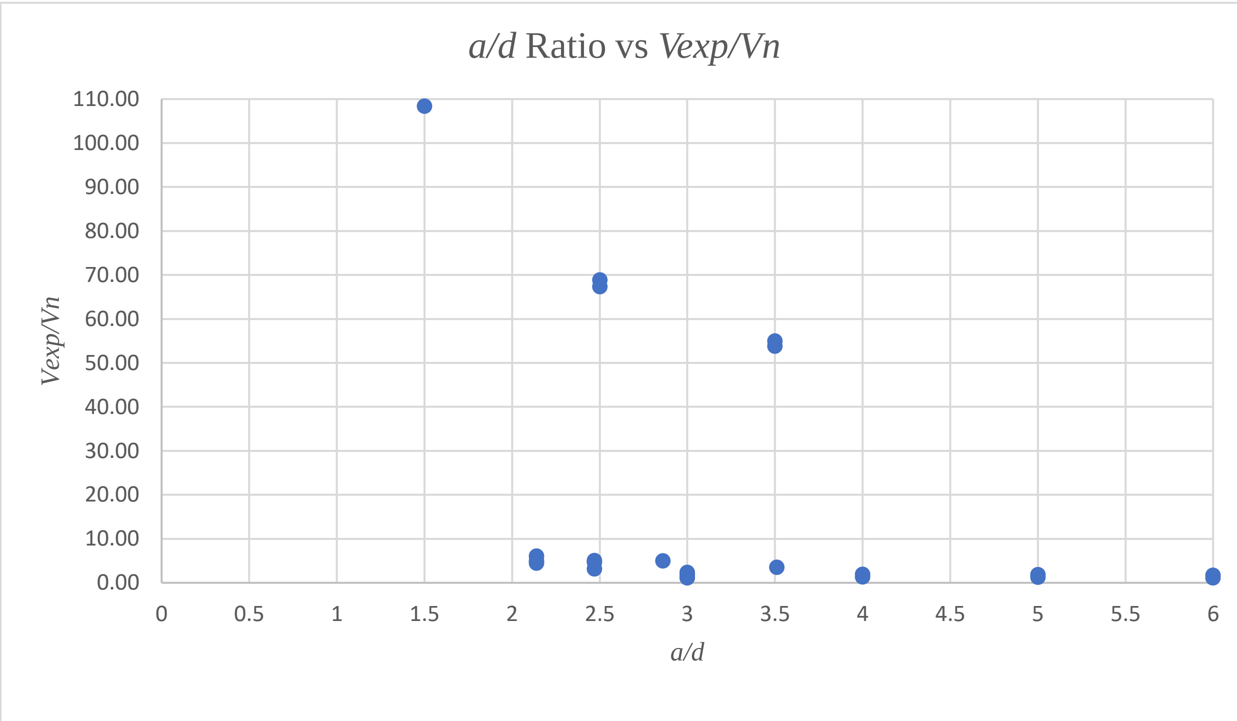

As shown in Figure 4.2, when the $^{a}/_{d}$ ratio was less than 1.5, the $^{V_{exp}}/_{V_n}$ was high due to arch action. Although the method used by ACI 440.4R cannot accurately compute for beams ranging below 1.5, the $^{V_{exp}}/_{V_n}$ is more accurate for beams with $^{a}/_{d}$ greater than 1.5. However, inconsistencies occurred between 2 and 3.5 because, as previously mentioned, the method neglected the longitudinal reinforcement and effects of the prestressing level as well as the stirrup ratio when beams are under-reinforced. This pattern of $^{a}/_{d}$ effect on shear capacity aligns well with conclusions from previous studies (Grace et al., Park and Naaman, Wang et al., and Nabipaylashgari), which found that arch action caused beams to fail in compression of concrete when the $^{a}/_{d}$ ratio was less than 1.5. On the other hand, when the ratio was greater than 1.5, the beams failed in tension or compression shear crack due to the beam's action.

The only parameter ACI 440.4R considers is the stirrup ratio, $^{A_v}/_{S}$. As the stirrup ratio increases – either by increased total area of the transverse reinforcement, decreased stirrup spacing, or both – the nominal shear capacity of the beams typically increases. For example, when calculating V_n for beams C100-C4-3 and C100-C8-3, with the same A_v of 0.18 in^2 but an S of 4 inches and 8 inches, respectively, the result was 28.4 kips and 14.2 kips. Similarly, when comparing beam C5 (A_v of 0.05 in^2 and S of 8 inches) to C7 (A_v of 0.1 in^2 and S of 4 inches), the V_n result was 11.1 kips and 15.9 kips, respectively. Results from Grace et al. and Wang et al. studies confirmed the effect of the stirrups spacing on $^{V_{exp}}/_{V_n}$ (Figure 4.3).

Figure 4.3. Comparison of S and V_{exp}/V_n (ACI 440.4R)

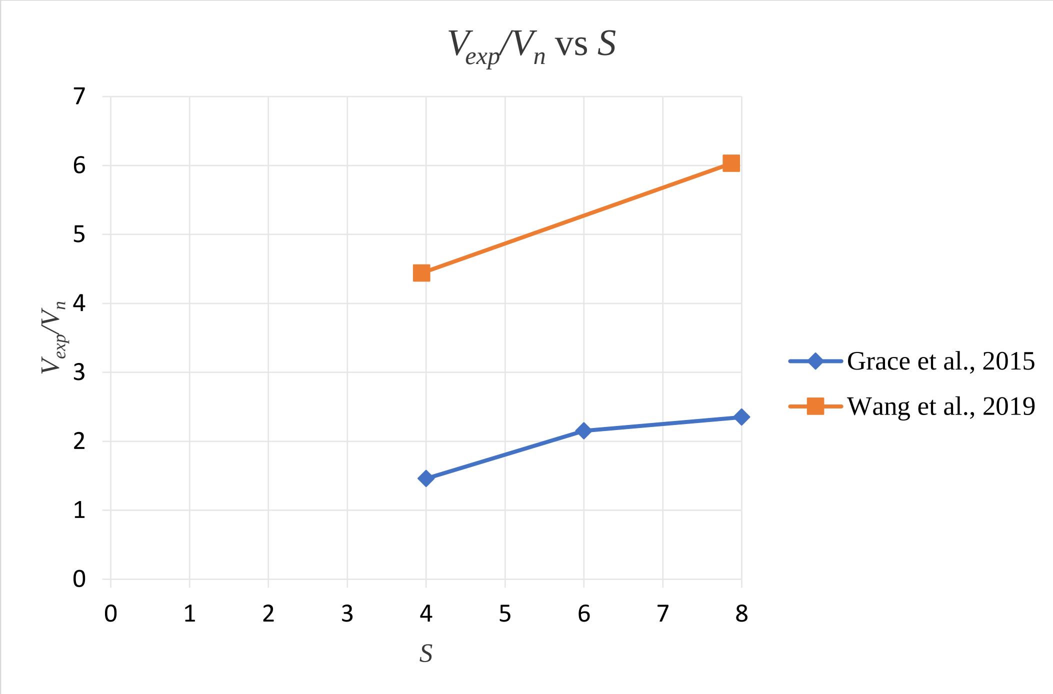

As shown in the figure, Grace et al.'s beams were C100-C4-3, C100-C6-3, and C100-C8-3 were reinforced with CFRP stirrups that had a total effective area of 0.18 in^2 but a *S* of 4 inches, 6 inches, and 8 inches, respectively. As the stirrups spacing increased the V_{exp}/V_n increased from 146, 2.15, to 2.35, respectively, resulting to a more conservative estimate to the nominal shear capacity of the reinforced concrete beams. This could also be observed in Wang et al. study were PCII-5 and PCII-6 beams that were reinforced with steel stirrups that had a total area of 0.087 in^2 but a *S* of 3.94 inches and 7.87 inches, respectively, the V_{exp}/V_n decreased from 8.95 to 6.11 kips, respectively. Thus, showing that the only parameter that effect the V_{exp}/V_n is the A_v/S.

The evaluation of ACI 440.4R guidelines showed that, for this method to accurately predict the nominal shear capacity, a beam must have a θ close to 45°, a/d ratio greater than 1.5, and sufficient transverse reinforcement because ACI 440.4R ignores effects from the prestressing level, the longitudinal strain of prestressed reinforcement, the a/d ratio, and change in θ. Therefore, by ignoring these parameters and assuming θ to be 45° and β to be 2, nominal shear capacity will always be conservative compared to the experimental shear strength of the beams. Despite these disadvantages, ACI 440.4R is an efficient user-friendly method with known variables that only need to be placed into the equations.

4.2 AASHTO 2018

Using the same specimens, the AASHTO 2018 guideline was also evaluated. The V_{exp}/V_n ratio is presented in Figure 4.4.

Figure 4.4. V_{exp}/V_n Ratio (AASHTO 2018)

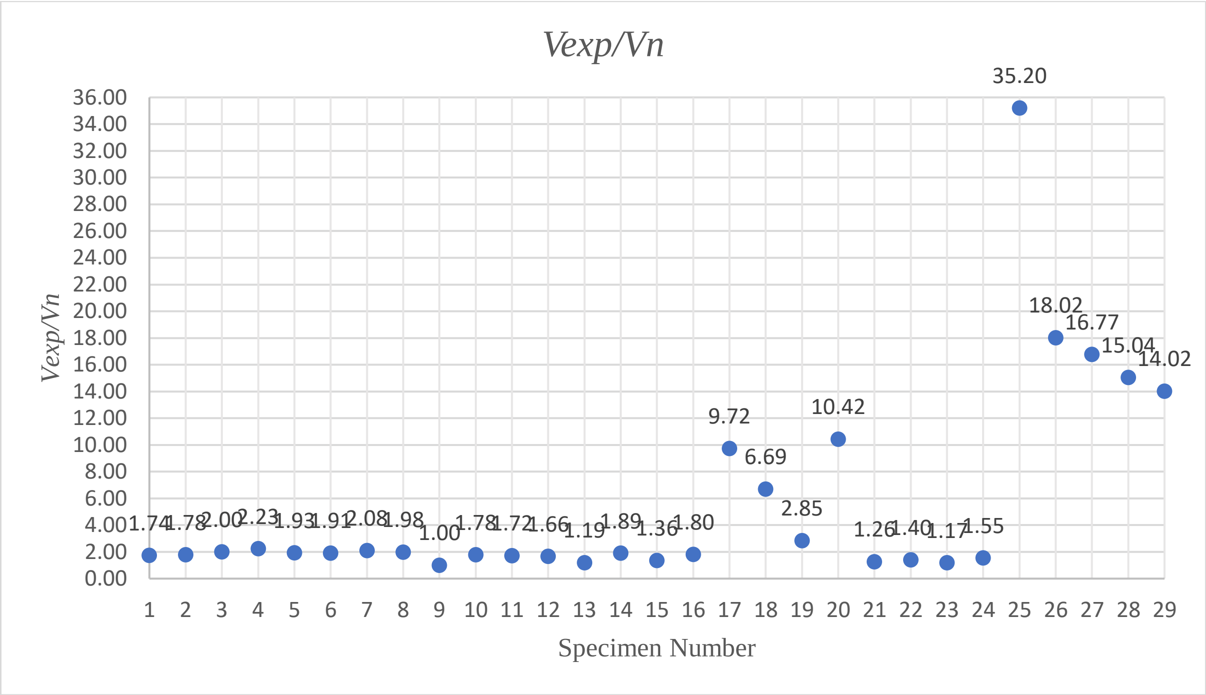

Figure 4.4 shows that the average V_{exp}/V_n ratio was equal to 5.59, with a minimum of 1.00 and a maximum of 35.20. Exclusive analysis of the V_{exp}/V_n ratio, however, could lead to the

conclusion that the AASHTO 2018 method is very conservative. Therefore, this study also compared the strain of the prestressing longitudinal reinforcement, ε_f, to the V_{exp}/V_n ratio to gain a clearer prediction of AASHTO 2018 (Figure 4.5).

Figure 4.5. Comparison of V_{exp}/V_n and ε_f (AASHTO 2018)

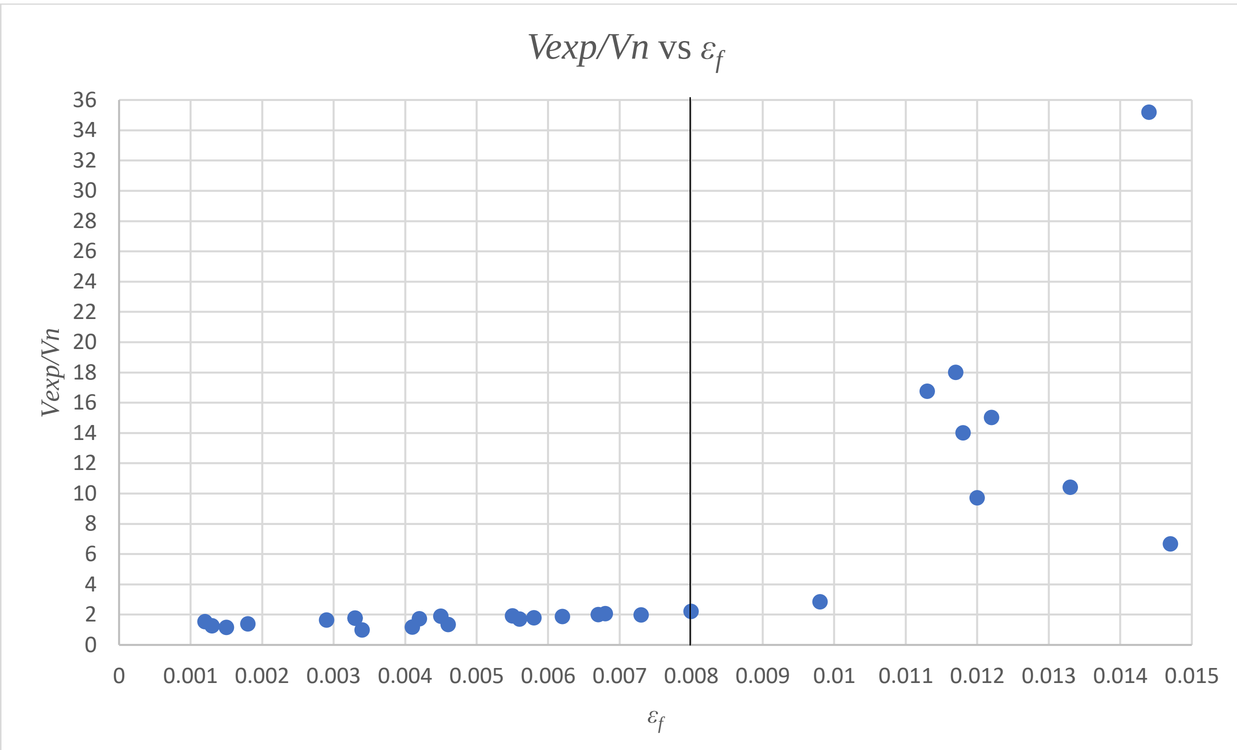

As shown in Figure 4.5, the specimens were partitioned into two sections depending on their respective ε_f to accurately compare the ε_f to the V_{exp}/V_n ratio. The first section included beams with $\varepsilon_f \leq 0.008$, specifically specimens 1–16 and 21–24, while the second section included beams with $\varepsilon_f > 0.008$, specifically specimens 17–20 and 25–29. Because the methodology of AASHTO 2018 is based on the SMCFT, ε_f plays a crucial role when calculating V_n since it affects both θ and β, as discussed in Section 3.2.3. According to the guideline, as the ε_f increases, θ also increases, causing the shear capacity of the stirrup, V_f, to decrease because as the shear crack becomes steeper it is resisted by fewer stirrups, making V_f smaller. Moreover, when ε_f decreases, θ also decreases, resulting in increased V_f because as the shear crack becomes shallow it is resisted by more stirrups, making V_f larger. This behavior is illustrated in Figure 4.6.

Figure 4.6. Equilibrium Diagram to Calculate Tensile Force in Reinforcement (Darwin et al., 2016)

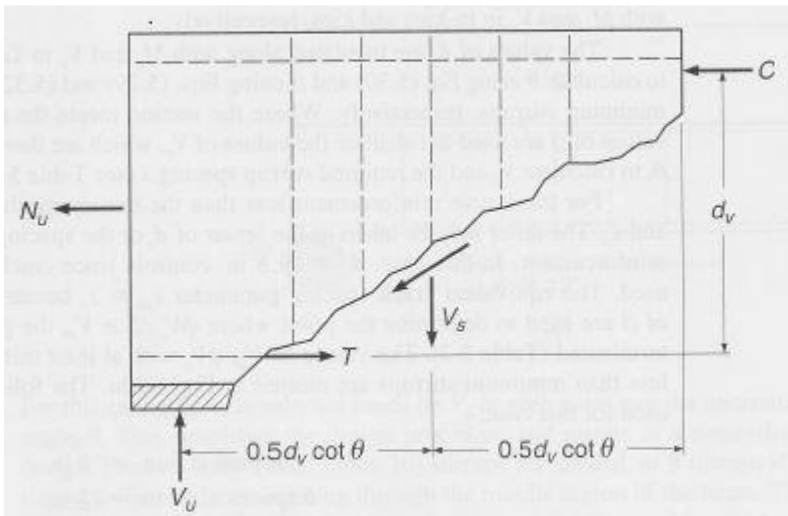

This study also compared the θ calculated for AASHTO 2018 and the experimental θ. Results showed that the θ for specimens with $\varepsilon_f \leq 0.008$ were very conservative, whereas the θ for specimens with $\varepsilon_f > 0.008$ were higher compared to their respective experimental θ. The results are presented in Table 4.3.

Table 4.3. Comparison of θ and θ_{exp} (AASHTO 2018)

#	Specimens	εf	Θ	Θ_{exp}	V_{exp}/V_n
1	C100-C6-3	0.0042	43.7	33-37	1.74
2	C100-C6-4	0.0033	47.7	27-46	1.78
3	C100-C6-5	0.0067	52.71	35-45	2
4	C100-C6-6	0.008	57.08	32-44	2.23
5	C100-S6-3	0.0055	44.9	32-36	1.93
6	C100-S6-4	0.0045	48.42	31-36	1.91
7	C100-S6-5	0.0068	52.79	38-47	2.08
8	C100-S6-6	0.0073	54.6	29-44	1.98
9	C100-C4-3	0.0034	40.1	32-45	1

10	C100-C8-3	0.0033	40.59	31-32	1.78
11	C100-S4-3	0.0056	48.76	29-38	1.72
12	C100-S8-3	0.0029	39.19	28-36	1.66
13	C072-C4-3	0.0041	43.52	37-39	1.19
14	C132-C4-3	0.0062	50.86	37-43	1.89
15	C072-S4-3	0.0046	45.12	28-38	1.36
16	C132-S4-3	0.0058	49.6	28-39	1.8
17	C5	0.012	71.41	-	9.72
18	C7	0.0147	75	-	6.69
19	C9	0.0098	63.34	-	2.85
20	C10	0.0133	75	-	10.42
21	PCII-3	0.0013	33.65	-	1.26
22	PCII-4	0.0018	35.41	-	1.4
23	PCII-5	0.0015	34.06	-	1.17
24	PCII-6	0.0012	33.21	-	1.55
25	PR-1.5-S	0.0144	75	43	35.2
26	PR-2.5-S	0.0117	70.2	30,44	18.02
27	PR-2.5-S	0.0113	68.58	32,44	16.77
28	PR-3.5-S	0.0122	71.97	19,31,36,45	15.04
29	PR-3.5-S	0.0118	70.31	22,30,41	14.02

The θ for beams with $\varepsilon_f \leq 0.008$ was higher than θ_{exp} because all the specimens were reinforced with prestressed tendons and non-prestressed longitudinal reinforcement. The inclusion of non-prestressed reinforcement in the beam resulted in the following, when the concrete cracked, tensile stresses were distributed between the prestressed tendons and the non-prestressed reinforcement, thereby alleviating of the stresses from the prestressing tendons and causing the ε_f to decrease. This relationship between ε_f and axial stiffness of the non-prestressed reinforcement, $E_f A_f$, is presented in equations (35) and (36), where $E_f A_f$ is in the denominator. For beams with $\varepsilon_f > 0.008$, θ was shown to be much higher than θ_{exp} because the beams were reinforced only with the prestressed tendons. This reliance on the prestressing tendons to resist all the tensile stresses when the concrete cracks resulted in an increase in ε_f, where all ε_f were extremely close to the ultimate strain capacity of the tendons, ε_{fu}.

The relationship between β and ε_f, shown in Figure 4.7, correlates well with figure 3.12 discussed in Section 3.2.3. As ε_f decreased, β increased, which increased the concrete compression stress section and consequently increased the concrete shear capacity, V_c. In contrast, when ε_f increased, β decreased, resulting in a smaller concrete compression stress section that decreased the concrete shear capacity, V_c. As shown in Figure 4.7, beams with $\varepsilon_f \leq 0.008$ had a β larger than 0.7, and beams with $\varepsilon_f > 0.008$ had a β smaller than 0.7. Comparing these results to Figure 4.5, the conclusion was made that beams with $\varepsilon_f \leq 0.008$ more accurately represent the V_c than beams with $\varepsilon_f > 0.008$.

Figure 4.7. Comparison of β and ε_f (AASHTO 2018)

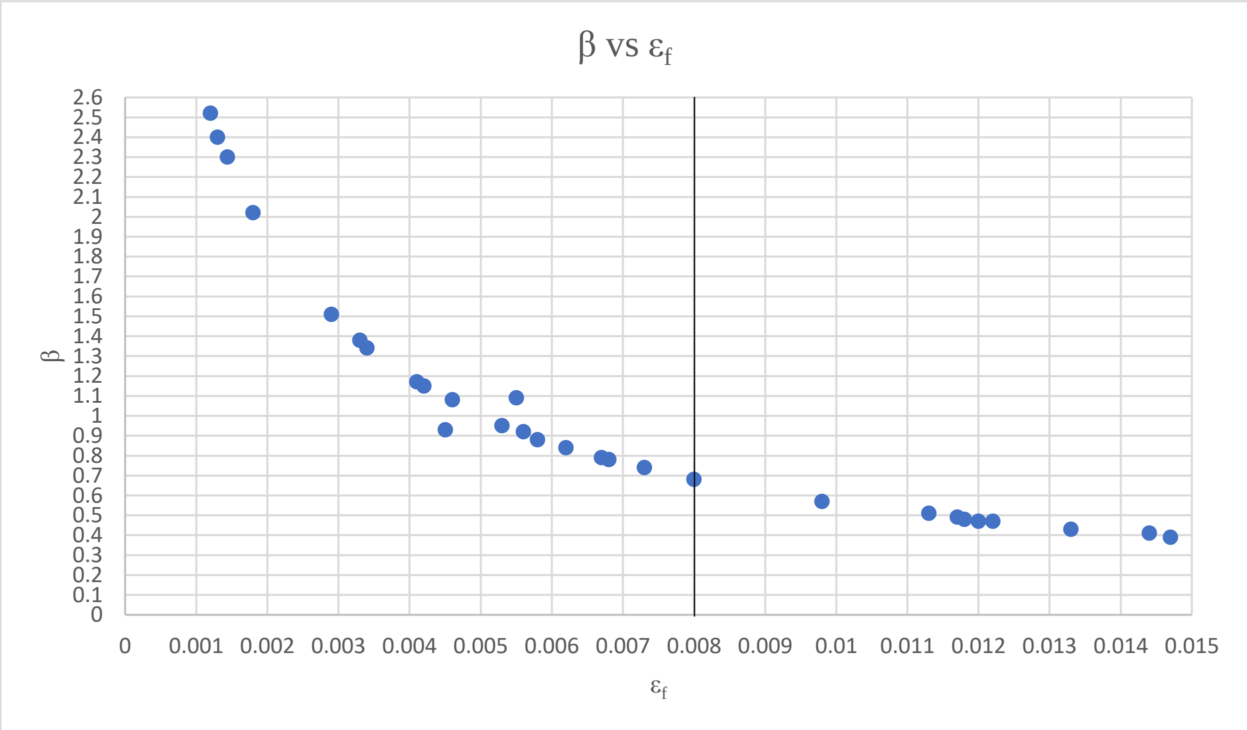

Results also showed that, although the prestressing level had a significant impact on the experimental shear capacity of the beams, it did not demonstrate the same impact when the nominal shear capacity was calculated. One reason for this difference could be that most beams were reinforced with only two prestressing tendons. If beams with multiple tendons were tested, a more noticeable impact on ε_f and V_n would be expected.

Results of the evaluation of AASHTO 2018 on the effect of the a/d ratio showed that changes in a/d impacted the result of V_n. For example, when comparing specimens 1–4, the a/d ratio was 3, 4, 5, and 6 and the V_n was 33.8, 29.3, 24.5, and 20.8 kips, respectively. Similarly, for beams 21–22, the a/d was 2.14 and 2.86 and the V_n was 12.03 kips and 10.75 kips, respectively. Overall, as the a/d ratio increased, V_n decreased due to the impact of the factored shear force, V_u, and the factored moment force, M_u, on the ε_f. As the shear span, a, increased, M_u increased, thereby increasing the tensile stress in the flexural tension region. This increase in tensile stress resulted in increased strain of the prestressed tendons, which consequently increased θ and decreased β and decreased the nominal shear capacity of the beam. Analysis of the effect of the a/d ratio on the V_{exp}/V_n ratio showed that beams with high a/d ratio and $\varepsilon_f \leq 0.008$ had low V_{exp}/V_n ratio, whereas beams with low a/d ratio and $\varepsilon_f > 0.008$ had high V_{exp}/V_n ratio (Figure 4.8).

Figure 4.8. Comparison of *a/d* Ratio and V_{exp}/V_n (AASHTO 2018)

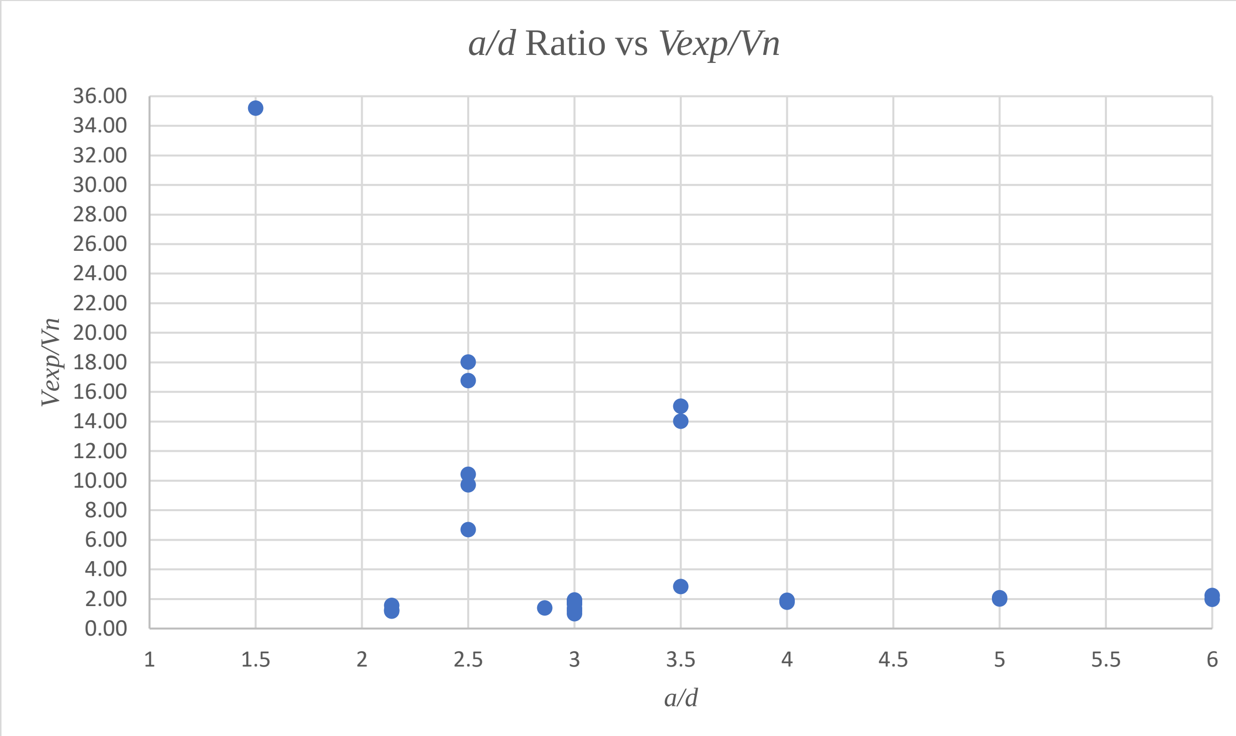

When $^a/_d$ was less than 1.5, the beam failed in concrete compression due to arch action that AASHTO 2018 neglected. However, for beams with $^a/_d$ higher than 1.5, AASHTO 2018 accurately computed the V_n of multiple beams, as shown in Figure 4.8. The divergence of some the data points was due to the effect of $\varepsilon_f > 0.008$ and its impact on both θ and β, as discussed previously. Analysis of the effects of the stirrup ratio, $^{A_v}/_S$, on the $^{V_{exp}}/_{V_n}$ ratio showed that sufficiently reinforced beams with $\varepsilon_f \leq 0.008$ had a low $^{V_{exp}}/_{V_n}$, whereas under-reinforced beams had a high $^{V_{exp}}/_{V_n}$, as shown in Figure 4.9. Additionally, $\varepsilon_f > 0.008$ noticeably distorted the $^{V_{exp}}/_{V_n}$.

Figure 4.9. Comparison of A_v/S Ratio and V_{exp}/V_n (AASHTO 2018)

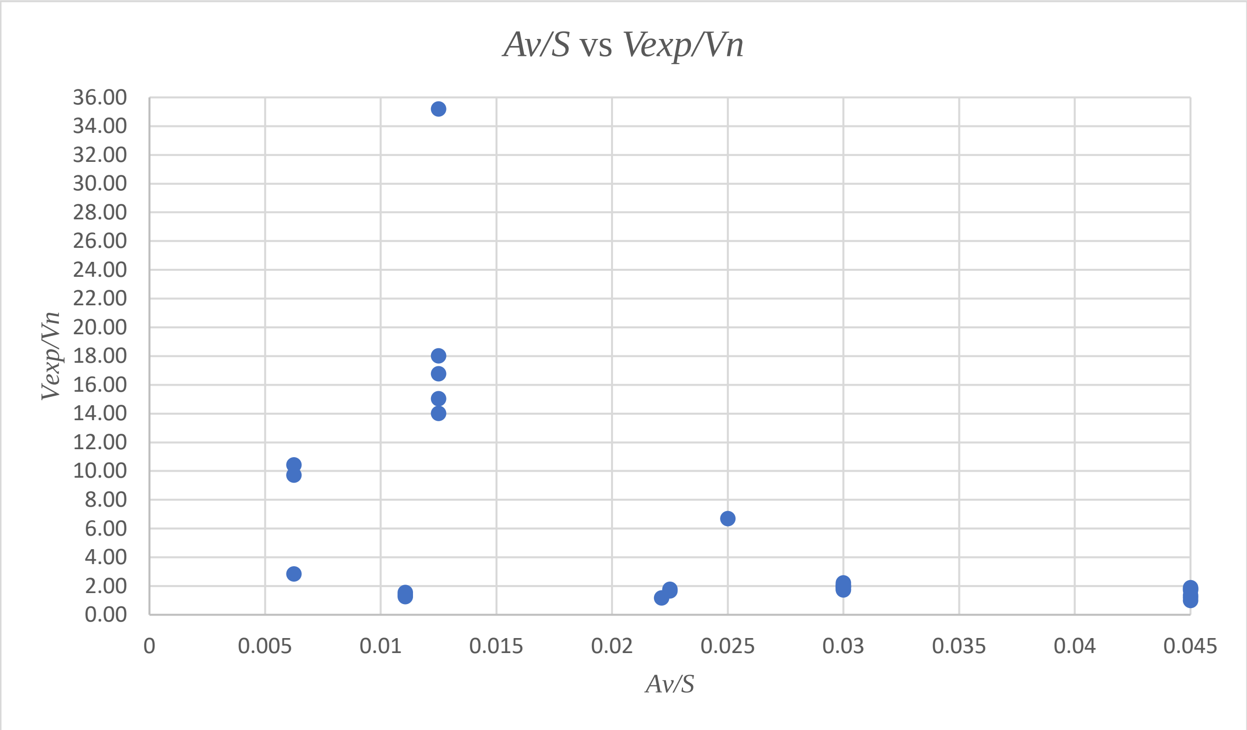

When computing the V_n, results showed that the V_n increased as the $A_v/_S$ increased, as shown with beam numbers 23 and 24 with stirrup spacing of 3.93 inches and 7.87 inches and nominal shear capacity of 16.95 kips and 11.88 kips, respectively. Notably, stirrup type had minimal impact on the shear capacity. For example, when comparing beam 4 reinforced with CFRP stirrup to beam 8 reinforced with steel stirrups, the V_n for beams 4 and 8 was 20.8 kips and 22.3 kips respectively. The effects of $A_v/_S$ and stirrup type were identical to conclusions from previous studies, as discussed in Chapter 2.

The evaluation of AASHTO 2018 methodology to calculate nominal shear capacity revealed ε_f to be the most influential parameter for the nominal shear capacity. If ε_f increased, θ increased and β decreased, causing V_f and V_c as well as V_n to decrease. However, if ε_f decreased, θ decreased and β increased, causing V_f and V_c as well as V_n to increase. Unfortunately, results showed that use of AASHTO 2018 means that θ and β are not calibrated for prestressed concrete beams reinforced with FRP since θ is higher than the experimental θ. Since both θ and β are dependent on ε_f, as elucidated in Section 3.2.3, β could exceed its current range.

The effect of the prestressing level was not noticeable when calculating V_n because most beams were reinforced with only two prestressing tendons, which could have reduced the effect of the prestressing level. However, the effect of the a/d ratio was clear since V_u and M_u are variables when calculating ε_f. Therefore, as a/d increased, both V_u and M_u increased causing ε_f to increase and V_n decrease. In addition, when a/d was less than 1.5, AASHTO 2018 could not accurately calculate V_n, but AASHTO 2018 produced more precise calculations when the a/d ratio was higher than 1.5. The effect of A_v/S was accounted for when calculating V_n since V_n increased when A_v/S increased. Despite its advantages, the accurate but conservative AASHTO 2018 method to calculate V_n is tedious and time-consuming due to required multiple variables and the varying nominal shear capacity along the span of the beam.

Chapter 5 – Conclusion

Fiber-reinforced polymer (FRP) can be effectively utilized as rods, sheets, bars, and tendons due to its high strength-to-weight ratio, non-corrosiveness, non-magnetic properties, and flexibility. FRPs include carbon fiber-reinforced polymers (CFRPs), aramid fiber-reinforced polymers (AFRPs), and glass fiber-reinforced polymers (GFRPs). Previous studies have investigated these materials under various load conditions and in a variety of structures, including prestressed concrete beams reinforced with CFRP, which has the highest tensile modulus out of all FRP varieties.

Previous studies have investigated the flexural behavior of beams reinforced with FRP, the shear behavior lacks accuracy in current design guides.

A literature review of the research for prestressed concrete reinforced with CFRP tendons under shear load revealed a consensus that the main parameters affecting the shear capacity of prestressed beams reinforced with CFRP are prestressing level, stirrup ratio, and shear span-to-depth ratio. In addition, an evaluation of the two U.S. design guidelines, ACI 440.4R-04 and AASHTO 2018, showed that, in order for the ACI 440.4R method to accurately predict nominal shear capacity, the beam must have θ close to 45°, ${}^{a}/_{d}$ ratio higher than 1.5, and sufficient transverse reinforcement. These factors are necessary because ACI 440.4R ignores effects from the prestressing level, the longitudinal strain of the prestressed reinforcement, the ${}^{a}/_{d}$ ratio, and changes in θ. Consequently, by ignoring these essential parameters and assuming θ equal to 45° and β equal to 2, ACI 440.4R's nominal shear capacity will always be conservative compared to the experimental shear strength of the beams. A method to improve ACI 440.4R approach is to adopt the ACI 318-19 approach. Although, ACI 318-19 needs to be calibrated for prestressed concrete beams reinforced with FRP, ACI 318-19 does include the effect of the prestressing level, $^{a}/_{d}$ ratio, $^{A_v}/_{S}$ ratio, and flexural and web shear crack making ACI 318-19 in theory more accurate than ACI 440.4R. However, tests and studies to prove that ACI 318-19 is more accurate than ACI 440.4R have not been conducted.

This study also evaluated the AASHTO 2018 method of calculating the nominal shear capacity. Results showed that the parameter ε_f most significantly affects the nominal shear capacity. If $\varepsilon_f > 0.008$, θ increases and β decreases, causing V_f and V_c to decrease, resulting in decreased V_n. If $\varepsilon_f \leq 0.008$, θ decreases and β increases, causing V_f and V_c to increase, resulting in increased V_n. However, use of AASHTO 2018 in its current state means that θ and β are not calibrated for prestressed concrete beams reinforced with FRP because calculated θ is higher than the experimental θ. Since both θ and β are dependent on ε_f, as described in Section 3.2.3, the β could be higher than necessary. Grace et al. (2015) modified the AASHTO LRFD simplified approach using their prestressed concrete beams reinforced with FRP. The compression of V_n to V_{exp} using the average $^{V_{exp}}/_{V_n}$ of 0.97 with standard deviation of 0.088, but more and varied reinforced beams samples are required to improve the modified AASHTO LRFD simplified method.

Finally, the objective of this thesis was to evaluate the shear strength determination guidelines in the ACI 440.4R-04 and AASHTO 2018 for prestressed concrete beams reinforced with CFRP tendons. Study results showed that both guidelines conservatively calculate the nominal shear capacity for prestressed concrete beams reinforced with CFRP tendons. Accurate prediction of the nominal shear capacity of the beams requires the beams to be confined to the limits of the respective guidelines. Consequently, more research on shear behavior of prestressed concrete beams reinforced with CFRP tendons is required to improve both guidelines. In future research, the beams should be reinforced only with CFRP tendons as tension reinforcement due to the unique behavior of prestressed CFRP tendons compared to prestressed steel tendons and non-prestressed reinforcement. In addition, parameters should vary between beams. As shown in Section 4.2, beams reinforced with only prestressed CFRP tendons had a high V_{exp}/V_n compared to beams with both prestressed CFRP tendons and non-prestressed reinforcement, where V_{exp}/V_n was close to 1.0. Therefore, more tests must be conducted on beams reinforced with only prestressed CFRP tendons using various prestressing levels, a/d ratios, and A_v/S ratios to create guidelines that more accurately predict the nominal shear capacity of prestressed beams reinforced with CFRP tendons. It has to be noted the purpose of these researches is to create guidelines that more accurately predict the nominal shear capacity and not to design beams without non-prestressed reinforcement. On the contrary, it is advised to provide non-prestressed reinforcements when designing prestressed concrete beams reinforced with CFRP to provide ductility to the concrete beams.

References

American Association of State Highway and Transportation Officials (AASTHO). (2018). *Guide specifications for the design of concrete bridge beams prestressed with carbon fiber-reinforced polymer (CFRP) systems* (1st ed.). AASHTO.

American Concrete Institute (ACI). (2004). *Prestressing concrete structures with FRP tendons*. ACI 440.4R-04. https://doi.org/10.1061/40753(171)160

Belarbi, A., Dawood, M., Poudel, P., Reda, M., Tahsiri, H., Gencturk, B., Rizkalla, S. H., & Russell, H. G. (2019). *Design of concrete bridge beams prestressed with CFRP Systems*. NCHRP. https://doi.org/10.17226/25582

Bentz,, E. C., Vecchio, F. J., & Collins, M. P. (2006). Simplified modified compression field theory for calculating shear strength of reinforced concrete elements. *ACI Structural Journal*, *103*(4), 614–624. https://doi.org/10.14359/16438

Collins, M. P., & Mitchell, D. (1997). *Prestressed concrete structures*. Response Publications.

Darwin, D., Dolan, C. W., & Nilson, A. H. (2016). *Design of concrete structures* (15th ed.). McGraw-Hill.

Dolan, C. W. (1990). Developments in non-metallic prestressing tendons. *PCI Journal*, *35*(5), 80–88. https://doi.org/10.15554/pcij.09011990.80.88

Dolan, C. W., & Nanni, A. (1993). *Fiber-reinforced-plastic reinforcement of concrete structures*. American Concrete Institute.

Dolan, C. W., Hamilton, III, H. R., Bakis, C. E., & Nanni, A. (2001). *Design recommendations for concrete structures prestressed with FRP tendons* (Vol. 1). FHWA.

Grace, N. F., & Bebawy, M. (2019). *Evaluating long term capacity & ductility of carbon fiber reinforced polymer prestressing and post tensioning strands subject to long term losses, creep, and environmental factors, and development of CFRP prestressing specifications for the design of highway bridges*. Lawrence Technological University.

Grace, N. F., Rout, S. K., Ushijima, K., & Bebawy, M. (2015). Performance of carbon-fiber-reinforced polymer stirrups in prestressed-decked bulb T-beams. *Journal of Composites for Construction*, *19*(3), 04014061. https://doi.org/10.1061/(asce)cc.1943-5614.0000524

JSCE. (1997). Recommendation for design and construction of concrete structures using continuous fiber reinforcing materials. *Concrete Engineering Series*, No. 23.

Mather, B., & Tye, R. V. (1955). *Plastic-glass fiber reinforcement for reinforced and prestressed concrete: Summary of information available as of July 1, 1955*. (Report No. 6-421, Report 1). USACE.

Wolff & Miesseler. (1989). New materials for prestressing and monitoring heavy structures. *Concrete International*, *11*(9), 86–89.

Nabipay, P., & Svecova, D. (2014). Shear behavior of CFRP prestressed concrete T-beams. *Journal of Composites for Construction*, *18*(2), 04013049. https://doi.org/10.1061/(asce)cc.1943-5614.0000450

Nabipaylashgari, M. (2012). *Shear strength of concrete beams prestressed with CFRP cables*. The University of Manitoba.

Park, S. Y., & Naaman, A. E. (1999). Shear behavior of concrete beams prestressed with FRP tendons. *PCI Journal*, *44*(1), 74–85. https://doi.org/10.15554/pcij.01011999.74.85

Pepper, L., & Mather, B. (1959). *Plastic-glass fiber reinforcement for reinforced prestressed concrete; Summary of information from 1 July 1955 to 1 January 1959*. (Report No. 6-421, Report 2). USACE.

PROSPECT FOR NEW GUIDANCE IN THE DESIGN OF FRP (CEN/TC250). (2016).

Rizkalla, S. H., & Tadros, G. (1994). First smart highway bridge in Canada. *Concrete International*, *16*(6), 42–44.

Vecchio, F. V., & Collins, M. P. (1986). The modified compression-field theory for reinforced concrete elements subjected to shear. *ACI Journal Proceedings*, *83*(2). https://doi.org/10.14359/10416

Wang, Z., Yao, Y., Liu, D., Cui, Y., & Liao, W. (2019). Shear behavior of concrete beams pre-stressed with carbon fiber reinforced polymer tendons. *Advances in Mechanical Engineering*, *11*(1), 168781401881687. https://doi.org/10.1177/1687814018816879

Wight, J. K. (2016). *Reinforced Concrete: Mechanics and Design, Seventh Edition* (7th ed.). Pearson.

Wines, J. C., Dietz, R. J., & Hawley, J. L. (1966). *Laboratory investigation of plastic-glass fiber reinforcement for reinforced and prestressed concrete*. (Report No. 2). USACE.

Zoch, P., Kimura, H., Iwasaki, T., & Heym, M. (n.d.). *Carbon fiber composite cables—A new class of prestressing members*. Transportation Research Board, 19.